INVESTIGATING THE EFFECT OF POROSITY ON ELASTIC MODULUS THROUGH FINITE ELEMENT ANALYSIS AND MOLECULAR DYNAMICS SIMULATIONS

By © Stephen M. Handrigan

A Thesis submitted to the

School of Graduate Studies in partial fulfillment of

the requirements for the degree of

Master of Engineering

Memorial University of Newfoundland

May 2019

St. John's Newfoundland

Abstract

The effect of porosity on elastic modulus was studied. First, a study with experimental load-deflection curve using Finite Element Analysis and beam theory, Euler-Bernoulli and Timoshenko, to investigate the effect of porosity on elastic modulus of a cantilever beam undergoing tip loading. It was determined that porosity amount and location affected the elastic modulus of a cantilever beam undergoing tip loading. Second, an investigation into the applicability of atomistic modelling of vacancies as a method of studying the effect of porosity on elastic modulus was completed for two materials, pure iron and iron-chromium. The study involved testing several force fields and parameter sets to determine accuracy and reliability of prediction. It was determined that vacancy amount did influence elastic modulus, with some force fields and parameter sets providing more accurate prediction in modulus and reduction in modulus due to vacancies. Results were compared to experimental data and Finite Element model from literature.

Acknowledgements

At this time, I would like to acknowledge several people who have helped me through this challenging and rewarding experience. First, to Dr. Sam Nakhla, whom without your continuous ongoing support and encouragement I could not have completed this work. You made yourself available whenever I required assistance and provided words of encouragement in times of doubt. Under your supervision I have become a much better engineer than I was prior. You instilled a need for constant improvement and continuous learning within me that has allowed me to successfully complete this degree and push the boundaries of what I thought I could do. Thank you for being a great supervisor, as through your supervision, I have developed unforgettable skills, gained great friendships, and developed a true understanding of my future endeavours.

To my parents, Ray and Judy Handrigan, from a young age you both taught me the importance of education without which I would never have reached this level in academia. I am thankful for your ongoing support. To Meghan Kirkpatrick, my best friend and partner, without your support and ongoing sacrifices this would not have been possible. Your words of encouragement for continuous self-improvement have helped me immensely.

To my coworkers, Liam and Ruby, your continuous support and assistance will not be forgotten; I will cherish our friendships throughout my career.

Finally, I would like to extend my gratitude to Suncor Energy, as without their financial support I would not have been able to pursue this degree.

Table of Contents

List of Tables

List of Figures

List of Abbreviations and Symbols

2D – Two-Dimensional

3D – Three-Dimensional

Å – Angstrom

BCC – Body-Centered Cubic

CAPEX – Capital Expenditure

EAM – Embedded-atom Method

FCC – Face-Centered Cubic

FE – Finite Element

fs - femtosecond

GPa – Gigapascal

HCP – Hexagonal-Close Packed

MEAM – Modified Embedded-atom Method

nA – nano-Ampere

nm – nanometer

ps - picosecond

ReaxFF – Reactive Force Field

SEM – Scanning Electron Microscope

μm – micrometer

° – Degree

1. Chapter 1: Introduction

1.1. Background of Porosity

Porosity, or small voids within a body, is of critical importance to study. Porosity has been shown to negatively impact the mechanical properties of materials, with several of these properties being directly related to the failure criteria of a material. Before quantifying the effect porosity has on mechanical properties, it must be determined which class of porosity is to be studied. Zhang and Wang [1] categorized porosity into three classes: 1) low porosity (less than 10% porous), 2) low to medium porosity (10 – 70% porous), and 3) high porosity (more than 70% porosity). The distinction into three classes has allowed the development of various models studying the effect of porosity on mechanical properties. Yang [2] showed that low porosity materials can be modelled under the assumption of no interaction between pores – in other words, the pores are sufficiently far enough apart that stress concentrations generated by individual pores are not felt by other pores. Due to this assumption, when determining the effect of porosity on elastic modulus in low porosity materials, the only parameter that must be studied is the total porosity, allowing the model to be independent of material properties. The overlapping spherical pore model, equation (1-1), developed by Gao et al. [3] does not include material properties, a model shown by Morrissey and Nakhla [4] to be the most accurate empirical model to predict the reduction of elastic modulus in low porosity materials in the elastic region.

$$E_{ss} = E_0 \left(1 - \frac{\phi}{0.652}\right)^{2.23} \quad (1\text{-}1)$$

For the other classes the interaction of pores cannot be neglected. As such, models developed to study low to medium and high porosity materials must include material specific parameters. According to Zhang and Wang [1], these materials were treated as a "structure system with the [ideal material] solid being treated as structural components […] and pores are regarded as empty space."

Prior to the distinction of porosity into classes and with a focus on experimentation, Romanova, Krimer, and Tumanov [5] showed that pores affect many mechanical properties. These pores decrease the ultimate strength, the yield stress, and fatigue life in cyclic bending. In [5], it was shown that the decrease in mechanical properties was exponential with increasing porosity percent. In addition, large decreases were observed in the presence of large pores, while less drastic reductions in mechanical properties were observed in combinations of small and large pores [5]. Romanova et al. [5] posit that as the number of pores or total pore volume increases it is more likely that individual pores are affected by stress concentrations, leading to crack initiation, propagation, and, ultimately, failure [5]. Discussing pore shapes and the affect they have on mechanical properties, Romanova et al. [5] stated that pores changed shape as size increased, noting that "small pores […] were spherical" and "large pores were […] irregular elongated shapes […] [acting] as 'internal notches' […] [increasing] […] stress concentration[s]." Lastly, Romanova et al. [5] concludes that "useful life […] decreases exponentially with

increase in porosity." It is evident from the conclusions of Romanova et al. [5] that porosity clearly affects the mechanical properties and lifecycle of a structure. As such, the effect of porosity on the mechanical integrity of a structure must be investigated to better understand the mechanical response and behaviour throughout the structure's lifecycle.

To study the effects of porosity on mechanical response of a structure without knowing pore distribution, Hardin and Beckermann [6] showed that the elastic modulus could be modelled "as a function into finite element simulations […] [resulting] in accurate stress-strain fields in the elastic regime." Being able to study the effect of porosity on the mechanical properties of a material or structure with finite element (FE) is of utmost importance. Without this conclusion, researchers and engineers would have to model individual pores within FE models to study the effect of porosity – a dramatic increase in the time required to study an area of interest.

From the prior discussion, it can be reasoned that a material with macroscale pores would possess less carrying-capacity than the same material with no pores. This is because the total area over which the force is carried is reduced with the presence of macroscale pores; thus, with less material the carrying-capacity is reduced. The same cannot be said, with confidence, for the effect of microscale pores.

Let's suppose that there is a porosity of 1% in two identical bodies of the same material. Now, let's have one body have several large macroscale pores which obviously reduce the total volume of the body, with a total porosity of 1%. Let the other body have millions of small microscale pores, still totalling 1% total porosity. It

is obvious that the large pores create stress concentrations and will reduce the carrying-capacity of the material. It is not as obvious, but can be inferred, that the millions of microscale pores will also have stress concentrations and thus should reduce the carrying-capacity of the body. Therefore, since the effect of large, macroscale pores is understood and known, then the effect of small, microscale pores must also be understood and known.

To study the effect of microscale pores, two approaches were developed. First, a macroscale FE model was built in Abaqus to quantify the effect of microscale porosity on the elastic modulus of a cantilever. Second, an atomistic-scale molecular dynamics simulation was performed to quantify the effect of vacancies on elastic modulus. It is postulated that a vacancy-based atomistic model would capture a similar effect to the macroscale FE model, in that the elastic modulus is reduced with increasing porosity (or vacancies). The purpose of this thesis is to provide justification for the use of simulations for the study of microscale porosity on elastic modulus and to demonstrate the usefulness of simulations.

1.2. Justification of Simulations

With the increase of computational power, more sophisticated modelling and simulation capabilities have been developed, allowing for more accurate calculations than previously performed for the determination of material properties and response. There are several benefits of performing computer-based simulations over physical experiments. Some of these benefits are purely economic, while others include the ease at which modifications can be performed and still be studied. For

example, when performing a simple uniaxial tension test, a load frame is required which is a high capital expenditure (CAPEX) item. As well, there are the financial and time expenses of preparing samples and performing the experiment. In addition, the financial and time costs of any one of these steps can increase dramatically if more accurate results are required or if modifications must be made to the equipment or samples. Conversely, performing a FE simulation of a uniaxial tension test requires a FE software package and a computer, both of which could be high CAPEX items, but are in general less expensive than a load frame. In addition, this method allows for easier manipulation of the remaining factors. Once a simulation has been developed, the efficiency of repeating the test with various parameters is much higher than physical experiments. In a simulation, if the material type or shape changes this is a much more simple, quick, and cost efficient adjustment when compared to physical experiments. As well, if the speed of testing must be adjusted, it too can easily be manipulated. In addition, computer scripts can be written which can automate the running of simulations to allow for less downtime and more efficient use of time. Lastly, small sources of error that are present in physical experiments, such as if the load frame has a slight rotation during the test, are removed. This error would not be present in a computer based simulation without being designed to do so, thus allowing for more accurate testing.

1.3. Thesis Overview and Purpose

The overall purpose of this Master's Thesis was to investigate the effect of porosity on the elastic modulus using FE Analysis and Molecular Dynamics simulations. To accomplish this, a 3D FE model was first built to allow for the study

of porosity amount and location on the elastic modulus of a cantilever beam undergoing tip loading. This model was built using experimental load-deflection results and Scanning Electron Microscope (SEM) images found in literature. Various porosity amounts were tested in various distributions throughout the length of the cantilever to study the influence porosity amount and location has on elastic modulus. After the FE model was completed, molecular dynamics simulations were used to study the effect of atomistic-scale vacancies on the elastic modulus. This study involved testing various force fields and parameters available in literature.

This thesis is written in manuscript format with four chapters. Chapter 1 provides the background information relevant to porosity's effect on the strength of a material as found in literature. Chapter 2 focuses on the analysis of a micro-cantilever beam using 3D FE Analysis. This study involved an in-depth analysis to first prove the use of FE Analysis and then apply it to the micro-cantilever beam found in literature. Chapter 3 involves an investigation into the applicability of atomistic-scale modelling using molecular dynamics simulations to determine effect of vacancies on elastic modulus. Chapter 3 involves studying several relevant force fields and parameter sets to determine the effect of vacancies on elastic modulus of a uniaxial tension test for two materials – pure iron, and iron-chromium. Finally, Chapter 4 summarizes the findings and provides an overview of the results of the two studies.

1.4. Co-authorship Statement

In the following sections of this thesis, some of the work was collaborative. As such, the author aims to outline the contributions made by the co-authors for each paper.

In the second chapter, the paper titled *A Finite Element Model to Study the Effect of Porosity Location on the Elastic Modulus of a Cantilever Beam*, contributions were made by Liam Morrissey. The design and identification of the research proposal, the practical aspects of the research, the data analysis, and the manuscript preparation was completed by the author of this thesis. Morrissey provided an Abaqus FE model of a two-dimensional cantilever to determine the relationship between reduction in modulus and porosity concentration. This is present in the section 2.3.4 Finite Element Model – Reduction in Modulus due to Porosity under Bending. As a result of completing this model, Morrissey also provided the written procedure for how the model was built, as well as the results provided from this model, which can be seen in section 2.4.2 Finite Element Model – Two-Dimensional Beam.

In the third chapter, the paper titled *A Molecular Dynamics Analysis of Atomistic-scale Vacancies in various metals to predict the Reduction in Elastic Modulus*, the author of this thesis is the only contributor.

References

1. E. Zhang and B. Wang, “On the compressive behaviour of sintered porous coppers with low to medium porosities—Part I: Experimental study,” *Mechanical Sciences*, vol. 47, *(4-5)*, pp. 744-756, April 2005.
2. F. Yang, “Size-dependent effective modulus of elastic composite materials: Spherical nanocavities at dilute concentrations,” *Applied Physics*, vol. 95, *(7)*, pp. 3516, January 2004.
3. X. Gao, T. Wang and J. Kim, "On ductile fracture initiation toughness: Effects of void volume fraction, void shape and void distribution," *International Journal of Solids and Structures*, vol. 42, *(18)*, pp. 5097-5117, 2005
4. L. S. Morrissey and S. Nakhla, “A finite element model to predict the effect of porosity on elastic modulus in low porosity materials,” *Metall and Mat Trans A*, vol. 40, pp.2622-2630, July 2018.
5. N. I. Romanova, G. S. Kreimer, and V. I. Tumanov, “Effects of residual porosity on the properties of tungsten carbide-cobalt hard alloys,” *Soviet Powder Metall Met Ceram*, vol. 13, pp. 670-673, August 1974.
6. R. A. Hardin and C. Beckermann, “Effect of porosity on the stiffness of cast steel,” *Metall and Mat Trans A*, vol. 38, pp. 2992-3006, December 2007.

2. Chapter 2: A Finite Element Model to Study the Effect of Porosity Location on the Elastic Modulus of a Cantilever Beam

Abstract: The effect of the location of porosity concentration on elastic modulus of a cantilever beam is investigated. First, one-dimensional investigation with beam theory, Euler-Bernoulli and Timoshenko, was performed to estimate the modulus based on load-deflection curve. Second, three-dimensional Finite Element (FE) model in Abaqus was developed to identify the effect of porosity concentration. The use of macro-models such as beam theory and three-dimensional FE model enabled enhanced understanding of the effect of porosity on modulus.

2.1. Introduction

2.1.1. Background

It is known that porosity affects the mechanical properties of metals. In many materials, increases in macroscale pore sizes have shown to decrease ultimate strength, yield stress, and fatigue life [1]. However, due to advancements in manufacturing, pores in metals tend to be on the microscale instead of macroscale. This presents new concerns since the effect on a material's mechanical properties due to this microporosity is unknown [2]. This is critical because without understanding how microporosity affects a material, the ability to predict behavior due to loading throughout its lifecycle is difficult. Throughout the life cycle of a structure, exposure to various environmental conditions, sometimes harsh, is possible. Due to these environmental conditions, it is possible that porosity can be increased in the material as shown by Morrissey, Handrigan, and Nakhla [3]. As such, structures may be affected in various locations, and in differing amounts, depending on the exposure to the environment. It is critical to understand if the location of porosity has an effect on a structure.

2.2. Purpose of Study

It is known that porosity has an effect on elastic modulus. The work of Morrissey and Nakhla [4] presented a literature review on existing models available in literature. These models, mostly empirical, describe the effect of porosity on elastic modulus. In their study, Morrissey and Nakhla [4] developed a two-dimensional

Finite Element (FE) model that successfully captured the effect of porosity on elastic modulus in tension.

In the current work, a three-dimensional FE model is developed to investigate the effect of porosity on elastic modulus in bending. The effects of uniform distribution and concentrated zones of porosity were investigated. All FE model results were compared to test data reported in literature.

2.3. Procedures

2.3.1. Understanding Experimental Setup and Data

The first step in this study was to examine experimental load versus deflection data for micro-cantilevers. For this study, the work by Gong [5] was first analyzed to understand the correct beam theory to apply for determining elastic modulus, as well as to develop the three-dimensional FE model. An experimental elastic modulus of 147 GPa is reported in [5] for beam 5. As well, Gong's three-dimensional FE model captured the trend of porosity reduction with an average error in prediction of +38% compared to experimental results.

It is reported in [5] that samples were heat treated such that an average grain size of 8-10 μm was obtained. From these samples, the micro-cantilevers were produced at the University of California, Berkeley (UCB) using a focused ion beam (FIB). The FIB was used to cut three trenches using a 7-15 nA beam current – forming a U-shaped trench that had a width of 20-30 μm and a depth of 10 μm. Then using a 1-3 nA beam current, the outline of the beam was refined. Lastly, the sample was rotated 45°, both clockwise and counter-clockwise, around the longitudinal axis of the

beam to allow for cutting of the triangular bottom of the beam. See Figure 2-1 for a schematic of the cross-section. After the microcantilever was manufactured, a MicroMaterials nanoindenter was used to apply loading at the microcantilever beam tip and report beam tip displacement as the load was applied. The load was applied with a displacement rate of 10 nm/s until fracture. Lastly, the depth of indentation into bulk material was removed from the measured deflection to ensure only the displacement due to bending is measured. A Scanning Electron Microscope (SEM) image of the microcantilever with the nanoindenter from [5] is shown in Figure 2-2.

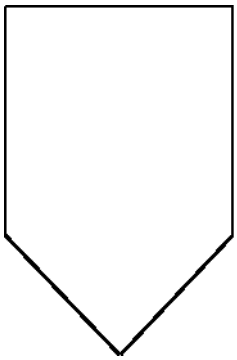

Figure 2-1 - Schematic of beam cross-section

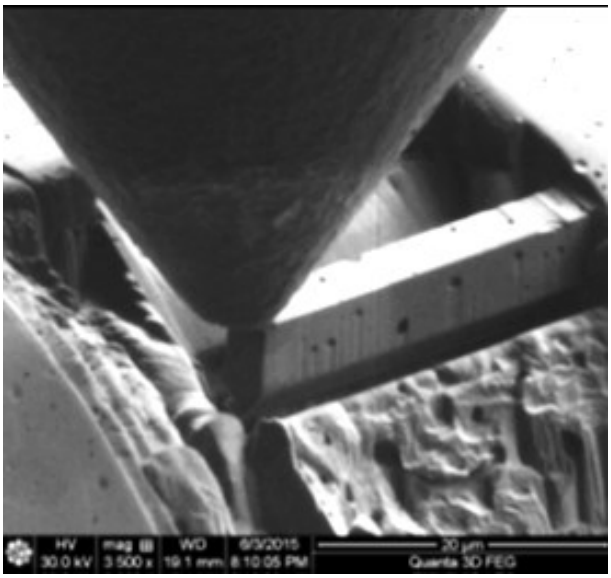

Figure 2-2 - SEM image of microcantilever and nanoindenter from [5]

2.3.2. Discussion of Beam Theory

To obtain the beam's elastic modulus from load-deflection data, two beam theories are chosen: Euler-Bernoulli beam theory and Timoshenko beam theory. The Euler-Bernoulli beam theory equation for the tip deflection of a cantilever due to an applied tip load is given by equation (2-1), while equation (2-2) provides the equation for Timoshenko beam theory.

$$\delta_{Tip-EB} = \frac{PL^3}{3EI} \tag{2-1}$$

$$\delta_{Tip-Timoshenko} = \frac{PL^3}{3EI} + \frac{PL}{\kappa AG} \tag{2-2}$$

In equations (2-1) and (2-2), P is the applied load, L is the length of the moment arm, E is the elastic modulus, A and I are the area and second moment of area of the cross-section, κ is the Timoshenko shear coefficient, and G is the shear modulus, given by the equation:

$$G = \frac{E}{2(1+\nu)}$$

where ν is Poisson's ratio.

It can be seen that the equations are similar with the exception that Timoshenko beam theory includes the deflection due to the shear force. To discuss the rationale of deciding between the two beam theories, one must understand the restrictions and assumptions of Euler-Bernoulli beam theory.

There are several restrictions for Euler-Bernoulli beam theory. The beam must: 1) undergo uniform bending, 2) have a high slenderness ratio (greater than 10:1), 3) be made of homogeneous material, 4) undergo symmetric loading through the width, and 5) possess a uniform cross-section. These restrictions lead to several assumptions: 1) plane cross-sections remain plane, 2) normal cross-sections remain normal, and 3) cross-section is rigid.

Euler-Bernoulli beam theory was developed for long, slender beams with a slenderness ratio of at least 10:1. At high slenderness ratios, the influence of shear deformation and stress are less pronounced and the assumptions of Euler-Bernoulli beam theory are holding. Meanwhile, for beams with low slenderness ratios, the effect of shear is more pronounced, violating the assumption on cross-section remaining normal to the neutral axis and making Timoshenko beam theory more efficient.

Before continuing the discussion comparing Euler-Bernoulli to Timoshenko beam theory, equations (2-1) and (2-2) have been re-written in equations (2-3) and (2-4), in terms of a rectangular cross-section, as shown in Figure 2-3, to clearly demonstrate the effect of slenderness ratio on deflection.

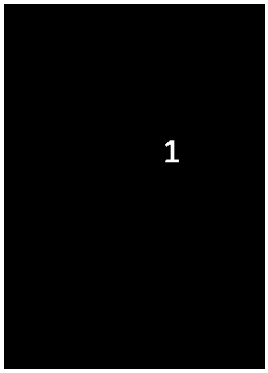

Figure 2-3 - Rectangular cross-section

$$\delta_{Tip-EB} = \frac{4P}{Eb}\left(\frac{L}{h}\right)^3 \tag{2-3}$$

$$\delta_{Tip-Timoshenko} = \frac{4P}{Eb}\left(\frac{L}{h}\right)^3 + \frac{P}{b\kappa G}\left(\frac{L}{h}\right) \tag{2-4}$$

As it can be seen from equations (2-3) and (2-4), slenderness ratio, the ratio between the length and height of the beam, clearly influences the deflection of the beam. It is known, and can be observed through equation (2-3) that beams of long, slender geometry will deflect more than short, stubby beams made of the same cross-sectional geometry and material. By observing Timoshenko's beam theory, equation (2-4), to study the effect of slenderness ratio, it can be seen that the first term has a cubic dependence on the slenderness ratio, while the second term, the shear effect term, has only a direct dependence on the slenderness ratio. As slenderness ratio increases, the second term becomes negligible compared to the first, and as a result it can be neglected, yielding to Euler-Bernoulli beam theory provided in equation (2-3). This clearly demonstrates what was stated prior – that at high slenderness ratios, the influence of shear deformation and stress are less pronounced; however, as slenderness ratio decreases and the beam becomes stubbier, the shear effect term is no longer negligible and can no longer be neglected. In addition, for materials weaker in shear, the shear effect is more pronounced and as such the contribution to deflection cannot be neglected. Thus, the effect due to shear must be included, at which point Timoshenko beam theory should be utilized.

Another factor for deciding between Euler-Bernoulli beam theory and Timoshenko beam theory is the boundary conditions. For a cantilever beam, Euler-Bernoulli beam theory was developed around the assumption that the beam has zero deflection, slope, and curvature at the root – no shear effect due to uniform bending restriction. A true cantilever is rigidly supported at one end, whereas the beam from [5] is not rigidly supported – the top face of the substrate is free to move. As such, the cantilever is not prevented from sloping at the root, thus another restriction for Euler-Bernoulli beam theory is violated. Timoshenko beam theory was not developed around this restriction, hence the reasoning for including the effect of shear on the beam.

Lastly, Euler-Bernoulli beam theory was developed under the restriction of uniform pure bending being applied to the beam, with no introduction of shear to the system. However, when a point load is applied to a beam, shear is introduced within the beam. As such, yet another restriction for Euler-Bernoulli beam theory is violated. As stated before, Timoshenko beam theory does not neglect the effect due to the shear force, and as such, the limitations of the applied load are not as strict as they are for Euler-Bernoulli beam theory.

A discussion on the geometry of the microcantilever is required to allow for critical analysis of the beam theory to which most confidence is held. Microcantilever beam 5 in [5] is approximately 7.5 μm tall, 4 μm wide, and 28 μm long. The load is applied at approximately 27 μm from the root – this will be taken to be the total length since deflection is also measured at this location. The cross-section is right-

pentagonal shaped, Figure 2-1, as proposed by Maio and Roberts in [6]. The authors believe the cross-section was chosen for the simplicity of manufacturing of the beams through the use of FIB cutting. From the dimensions provided in [5], the beam is considered to be short and stubby with a low slenderness ratio. As well, observing Figure 2-2, it is evident the beam is not undergoing uniform bending since the indenter acts as a concentrated, point load – this type of load, as discussed earlier, introduces shear into the cantilever. Lastly, continuing observations of the microcantilever, it can be stated that the microcantilever is not rigidly supported at the root. Due to these factors, shear effects may be highly pronounced, especially at the root, as such, both Euler-Bernoulli and Timoshenko beam theories were compared in the current study.

The next step in the analysis was to study the load-deflection curve in [5]. From the slope of the load-deflection curve, the elastic modulus was estimated using both Euler-Bernoulli and Timoshenko beam theory. To perform this calculation, equations (2-1) and (2-2) for Euler-Bernoulli and Timoshenko beam theory were re-written in terms of the load-deflection ratio, as shown in equations (2-5) and (2-6).

$$\frac{P}{\delta_{Tip-EB}} = \frac{3EI}{L^3} \tag{2-5}$$

$$\frac{P}{\delta_{Tip-Timoshenko}} = \frac{3EI\kappa AG}{3EIL + \kappa AGL^3} \tag{2-6}$$

Now that a clear understanding of the two beam theories has been developed, a discussion on the assumptions made for this study is provided.

2.3.3. Assumptions

For this study, several assumptions are made. Uranium Dioxide is highly anisotropic [7, 8]; however, it is assumed that the material acts as an isotropic material since the microcantilevers are ideally contained within a single crystal-grain. It is reported in [5] that not all microcantilevers are within a single grain; however, without additional information on number of grains and grain orientation, the assumption will remain. The FE model assumes the beam is solid, homogeneous and has a constant cross-section free of imperfections. As well, the FE model assumes uniform porosity distribution across the cross-section. Lastly, it is assumed that the effect on Poisson's ratio for porosities less than 5% is negligible [9, 10].

2.3.4. Finite Element Model – Reduction in Modulus due to Porosity under Bending

To accurately understand the effect of porosity on elastic modulus of a cantilever in bending, a FE model must be studied. The work of Morrissey and Nakhla [4] demonstrated that, when in tension, the effect of pores in low porosity materials, when voids do not interact, can be accurately modelled using relationships that account only for pore volume. However, during bending, the top and bottom portion of the beam are in different states of stress – one is in tension, while the other is in compression. Therefore, for a model to be able to be used for bending, it must also be accurate in both tensile and compressive loading. To validate the model for bending, the model developed by Morrissey and Nakhla [4] was tested under a compressive

load. Within this model, a macroscopic plate with a consolidated pore, representing various total porosities, is placed under loading and the slope of the resulting stress-strain curve is then used to determine a reduced modulus compared to the nominal modulus. Results from this model were then compared to the Gibson and Ashby model [11], a commonly referenced model to predict the elastic modulus of open- and closed-cell foams under compression (equations (2-7) and (2-8), respectively).

$$\frac{Ereduced}{Eperfect} = \left(\frac{\rho_f}{\rho_s}\right)^2 \tag{2-7}$$

$$\frac{Ereduced}{Eperfect} = \phi\left(\frac{\rho_f}{\rho_s}\right)^2 + (1-\phi)\frac{\rho_f}{\rho_s} \tag{2-8}$$

where ρ_f is the density of the porous material, ρ_s is the density of the solid material, and ϕ is the fraction of solid contained in the cell edges (taken as 0.9 in this case).

Referring to Figure 2-4, the results from the Morrissey and Nakhla [4] model showed strong agreement with the Gibson and Ashby model. Results were between the predicted values for open- and closed-cell foam with ϕ of 0.9. Therefore, since the Morrissey and Nakhla [4] model is accurate in both tension and compression, it can be used to approximate bending of a porous material.

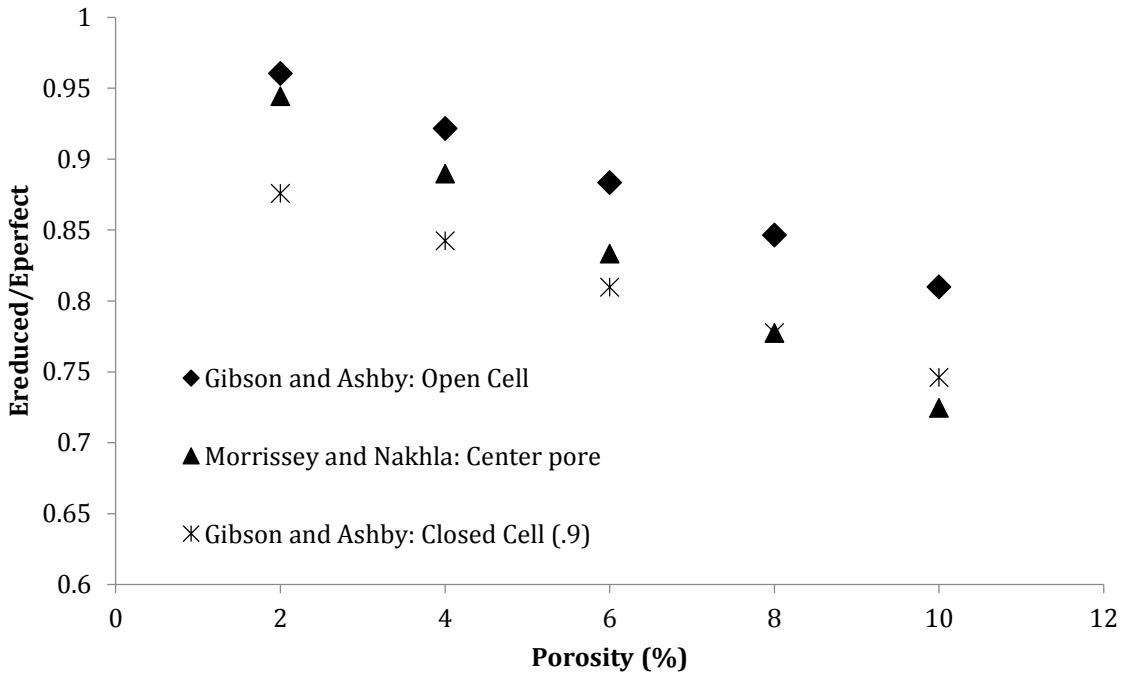

Figure 2-4 - Comparison of Morrissey and Nakhla [4], and Gibson and Ashby [11] compression models

After verifying the validity of the model for bending, a FE model was developed in Abaqus to test the effect of pore volume on the reduction of elastic modulus. For the FE model, a long, slender beam with a slenderness ratio of 10:1 was placed under bending using a concentrated tip load, as shown in Figure 2-5. Since it is a cantilever beam undergoing tip loading, it is known that the normal stress will vary along the beam length. As such, the location of porosity will likely factor into the reduction of elastic modulus and thus the model must be tested not only for pore volume, but also pore location. From the FE model, the resulting slope of the load-deflection curve was then used to determine the elastic modulus. First, a non-porous beam with a nominal modulus of 200 GPa was placed under loading. As expected, the resulting slope of the load-deflection curve provided the nominal modulus. Next, a consolidated spherical pore representing total porosities of 2.5% and 5% was placed at various locations

along the length of the beam. The beam was loaded as before and the modulus of elasticity for each case was calculated from the slopes of the resulting load-deflection curves. These values were then compared against the original nominal modulus to obtain a percent reduction in elastic modulus as a function of pore location along the beam length for both 2.5% and 5% porosity.

Figure 2-5 – FE Model undergoing Bending

2.3.5. Finite Element Model – Three-Dimensional Beam

With an understanding of how porosity amount and location affects the elastic modulus of a cantilever beam undergoing tip loading, a FE model to replicate the experimental setup must be completed. To build the FE model, a three-dimensional, deformable solid part was created in Abaqus. The substrate was sketched and extruded to create a cube. From the front face, the geometry was sketched and extruded to create the beam. The actual beam from [5] and the currently developed FE model are shown in Figure 2-6. The beam and substrate were then partitioned to allow for separate modification of material properties and mesh development. The beam was further partitioned into three segments of equal length, shown in Figure 2-7. This allows for different material properties to be applied to each segment.

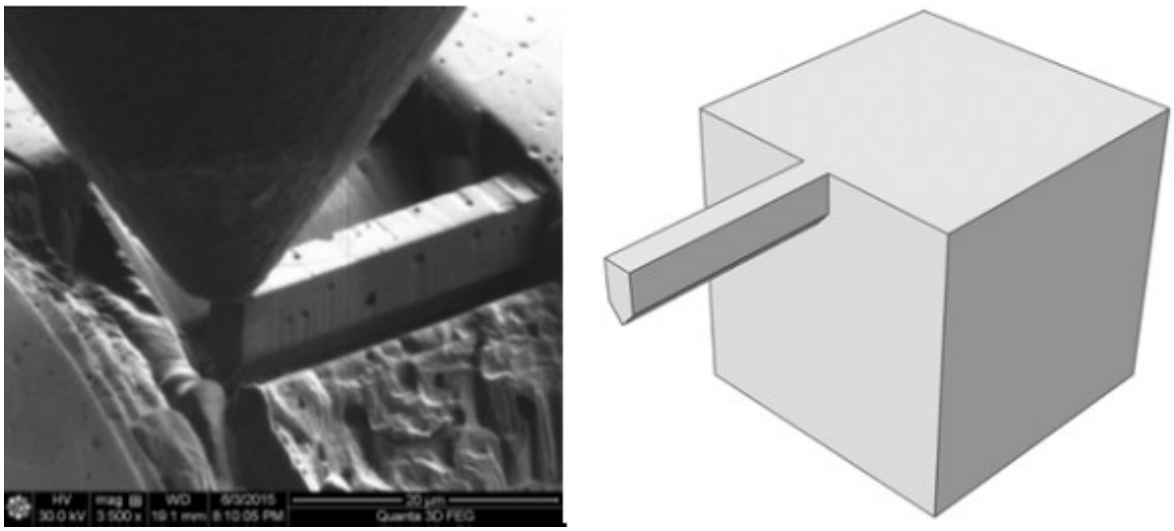

Figure 2-6 - SEM Picture of Experimental Setup [5] (left), Abaqus FE model this study (right)

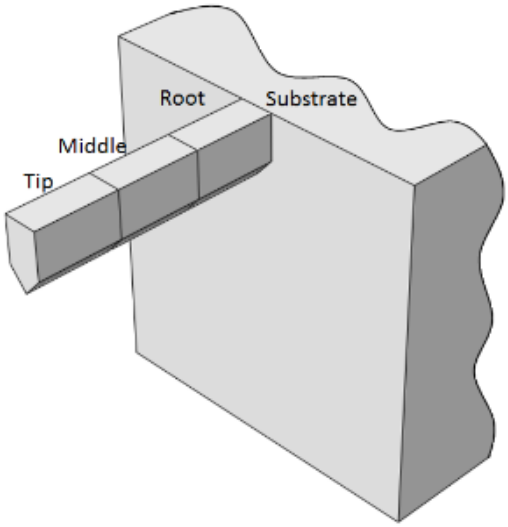

Figure 2-7 - Beam Sections (From left to right: Tip, Middle, Root, Substrate).

The next step was to develop the mesh. The mesh was refined differently within the beam than the substrate. The beam had 11,088 3D stress hex quadratic reduced integration elements, while the substrate had 4,464 3D stress hex quadratic reduced integration elements.

After this, boundary conditions are applied to the FE model. The side, rear, and bottom faces of the substrate have fixed boundary conditions, while the top and front faces, as well as the beam itself, are free surfaces, as shown in Figure 2-8 (lighter colors indicate free surfaces while darker indicate fixed surfaces). Next, a tip load was applied to the beam. Since the applied load may deform and create an indentation in the top surface where it is applied, the deflection is measured from the bottom side, directly under the location of the applied load. This ensures that the deflection data excludes the amount of indentation into the top of the beam to allow for more accurate calculation of the elastic modulus.

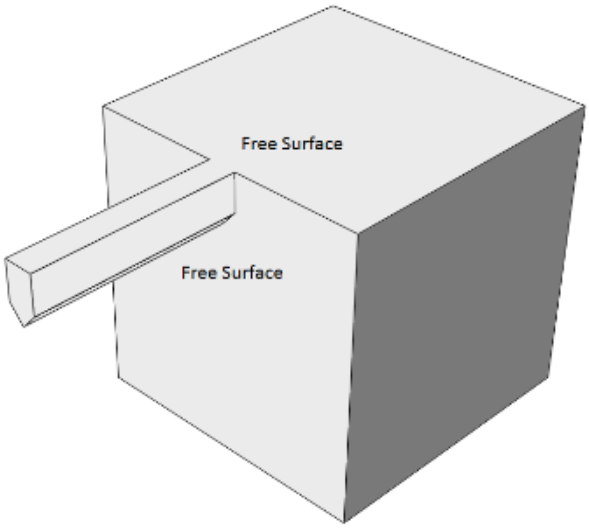

Figure 2-8 - Boundary Conditions (Top, Front, and Beam are free surfaces; all other sides fixed).

Before continuing the analysis, the size of the substrate must be determined such that its size does not cause stiffening of the beam due to the applied boundary conditions. However, before proceeding to substrate sizing, the magnitude of error in prediction due to a three-dimensional analysis must first be known.

An analysis was completed to determine the apparent reduction in modulus due to the three-dimensional analysis. First, a two-dimensional rectangular beam was analyzed using Euler-Bernoulli elements in Abaqus. Next, a three-dimensional analysis was completed using the same beam profile using 3D stress elements. Figure 2-9a shows the geometry of the 3D FE model. For each case, the modulus is calculated using load-deflection data and is normalized with the nominal modulus of 200 GPa. As can be seen from Table 2-1, the two-dimensional analysis, with a convergent mesh, is insensitive of the slenderness-ratio so it is able to return the nominal modulus. However, the three-dimensional analysis is sensitive to the effect of slenderness ratio. The three-dimensional analysis includes Poisson's effect – some of the energy is being stored in cross-sectional deformation (Poisson's contractions) instead of deflecting the beam and, as such, the prediction of modulus is slightly off. The beam studied in [5] has a slenderness ratio of less than four, so by completing a three-dimensional FE study, there may be large errors when using Euler-Bernoulli beam theory to calculate the elastic modulus. To continue the analysis, a three-dimensional analysis must be conducted to determine geometric effects on modulus prediction.

Table 2-1 - Comparison of Two-Dimensional and Three-Dimensional Analysis

Slenderness Ratio L/h	Two-Dimensional E(Euler)/E0	Three-Dimensional E(Euler)/E0
2	1	0.865
5	1	0.983
10	1	0.999
20	1	1.002

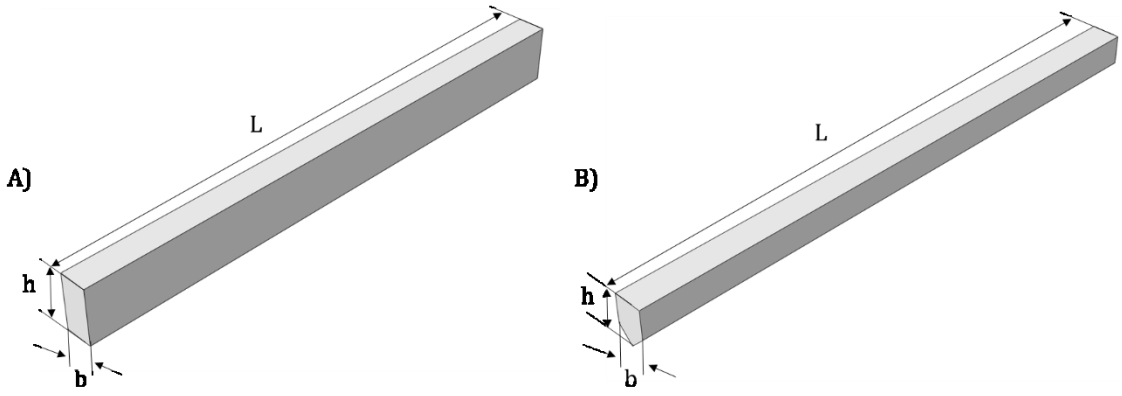

Figure 2-9 – Geometry of 3D Beam A) Rectangular, B) Right-pentagonal

Next, a study was completed to determine the apparent reduction in modulus due to beam geometry. As stated previously, the beam is short and stubby with a low slenderness ratio and the effect of this geometry on modulus must be studied as well. To perform this study, two beams were studied with slenderness ratios ranging from 2 to 20, one with a rectangular profile and the other with a right-pentagonal profile similar to [5] and [6]. Figure 2-10 shows the cross-sections studied while Figure 2-9 shows the geometry of the model for rectangular and right-pentagonal cross-sections.

Figure 2-10 - Rectangular and Right-Pentagonal Cross-section

Using a nominal modulus of 200 GPa, the apparent reduction in modulus due to geometry was determined, as shown in Table 2-2. The modulus was calculated using the load-deflection data from the FE models using both Euler-Bernoulli and Timoshenko beam theory, equations (2-5) and (2-6), respectively. Next, the modulus for each was normalized with the nominal modulus to determine the accuracy of prediction. It is apparent that as the slenderness ratio, L/h, increases, the normalized modulus for each beam approaches unity, in other words, the modulus predicted from the FE models approach the nominal modulus, thus recovering the true strength of the beam. However, it is evident that large errors in prediction exist for beams with low slenderness ratios when using Euler-Bernoulli beam theory – an error of 14% under prediction for the rectangular beam profile and almost an error of 10% under prediction for the right-pentagonal beam profile. Conversely, when using Timoshenko beam theory, the modulus is being slightly over-predicted (approximately +3% and lower). Due to the errors shown, care must be taken when determining the modulus of a beam in three-dimensional analysis. As stated before, the slenderness ratio of the beam studied in [5] was less than four and as such, potentially large errors are present in calculating the modulus.

Table 2-2 - Reduction in Modulus due to Geometry

	Rectangular Beam		Right-Pentagonal Beam	
L/h	E_{Euler}/E_{nom}	E_{Timo}/E_{nom}	E_{Euler}/E_{nom}	E_{Timo}/E_{nom}
2	0.865	1.0307	0.908427319	1.0250
5	0.983	1.0135	0.991312249	1.0117
10	0.999	1.0069	1.000915188	1.0061
20	1.002	1.0035	1.001792239	1.0031

After these studies were completed, the calculated modulus of a perfect beam with nominal modulus of 219 GPa and zero porosity was required. This was to provide a baseline for the predicted modulus due to the boundary conditions alone. As stated prior, it was unsure if the size of the substrate would have an effect on the results and as such, the FE model was first tested with various substrate sizes before testing porosity concentration and location.

For simplicity, the substrate was constrained to be a solid cube to reduce the number of variables that would have to be varied. Four substrate sizes were considered and the dimensions were scaled due to the beam's largest cross-sectional dimension – height. A schematic of the FE model with labels is shown in Figure 2-11. Substrate sizes were labelled A through D, with A being the smallest and D the largest. Substrate size A was approximately the same size as the height of the beam – an 8 μm x 8 μm x 8 μm cube. Substrate sizes B, C, and D were approximately one-and-a-half times (15 μm x 15 μm x 15 μm), three-times (20 μm x 20 μm x 20 μm), and six-times (40 μm x 40 μm x 40 μm) larger than the beam height, respectively. With each substrate size, the model was tested under constant tip load and the load-deflection data was used to calculate an elastic modulus. It should be noted that for a fully restrained cantilever, with no porosity, the nominal modulus should be returned; however, it is expected that a lesser modulus will be calculated due to the non-ideal boundary condition at the root of the beam.

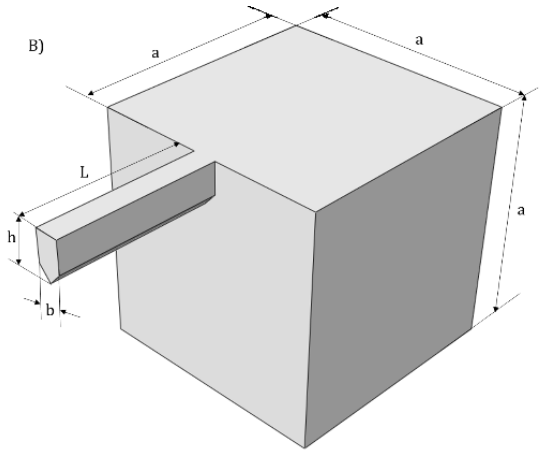

Figure 2-11 - Geometry of 3D FE Model

A comparison of the modulus obtained for each of the four cases is shown in Table 2-3. As can be seen, the size of the substrate does affect the response of the beam; however, as long as the substrate is at least three-times the height of the beam, the effect is insignificant. This is expected since when the substrate is small, the fixed boundary condition has a greater effect on the rigidity of the root of the beam since the stresses that propagate through the substrate do not sufficiently diminish before reaching the fixed boundary condition, thus effectively stiffening the beam and over-predicting the modulus. As the substrate size is increased, this effect is reduced to a point such that the modulus is unchanged since the fixed boundary condition is sufficiently far enough away from the root of the beam allowing the stresses to diminish, thus allowing for accurate modelling of the experimental setup. For this study, Substrate size D was chosen for the final 3D FE model to ensure the fixed boundary condition did not influence the results.

Table 2-3 - Comparison of substrate size

Substrate Size	Modulus Calculated (GPa)	% Reduction from Nominal
A	186.7	-14.7
B	182	-16.9
C	180	-17.8
D	180	-17.8

With the size of the substrate determined, it can be observed that due to the non-ideal boundary conditions, the calculated modulus from the load-deflection data is 18% less than the nominal modulus for the perfect, non-porous beam. This apparent reduction in modulus will become the base case to which the models with porosity will be compared. The justification is to isolate the effect of porosity and porosity location on reducing the modulus and clearly describe the effect on elastic modulus. If comparisons are made to the nominal modulus, the apparent reduction in modulus due to non-ideal boundary conditions (-18%) is included, thus the reduction in modulus due to porosity and porosity location is not clearly presented.

After the base case was developed, the percent reduction values determined in the previous section from the 2D FE model were applied to the nominal elastic modulus for Uranium Dioxide and a new modulus was calculated for when porosity is concentrated within different sections of the beam. A similar process was completed for when the porosity is uniformly distributed over the entire length of the beam. In this case, the percent reduction was approximately equal to the reduction experienced when porosity was concentrated at the tip for both porosities.

Next, the reduced modulus for each case was imported into the 3D FE model for the various setups. The reduced modulus for each case was applied to specific sections of the beam where the porosity was to be concentrated while the remaining sections of the FE model, including the substrate, were considered to be equal to the nominal modulus of 219 GPa for Uranium Dioxide [12].

2.4. Results And Discussion

2.4.1. Determination of Elastic Modulus from Experimental Data

Using the load-deflection curve reported in [5], the data was extracted and the slope for the linear section was determined to be approximately 1932 N/m. Next, the elastic modulus was calculated using both Euler-Bernoulli and Timoshenko beam theory from equations (2-5) and (2-6), resulting in 148 GPa and 154 GPa, respectively. This is compared to the reported modulus in [5] in Table 2-4.

Table 2-4 - Comparison of Calculated Modulus

Beam Theory	This Study	Reported in [5]
Euler-Bernoulli	148 GPa	147 GPa
Timoshenko	154 GPa	-

The authors believe that Timoshenko beam theory is the most accurate simply because of the inclusion of the effect due to shear. The justification for this is that the beam has a low slenderness ratio (less than four), the beam is not rigidly supported at the root, and the applied point load introduces shear into the beam, all three of which violate the restrictions of Euler-Bernoulli beam theory. As such, Timoshenko beam theory will be used to calculate the elastic modulus within this study.

2.4.2. Finite Element Model – Two-Dimensional Beam

Figure 2-12 and Figure 2-13 show the load-deflection curves for the cantilever beam with porosities of 2.5% and 5% at various locations along the length, respectively. As it can be seen, there is a clear effect on the elastic modulus as the porosity increases and as the porosity location is moved towards the root. From the slope of the load-deflection curves, the elastic modulus was calculated for each case using Timoshenko beam theory, equation (2-6), and was then compared to the nominal modulus inputted into the model.

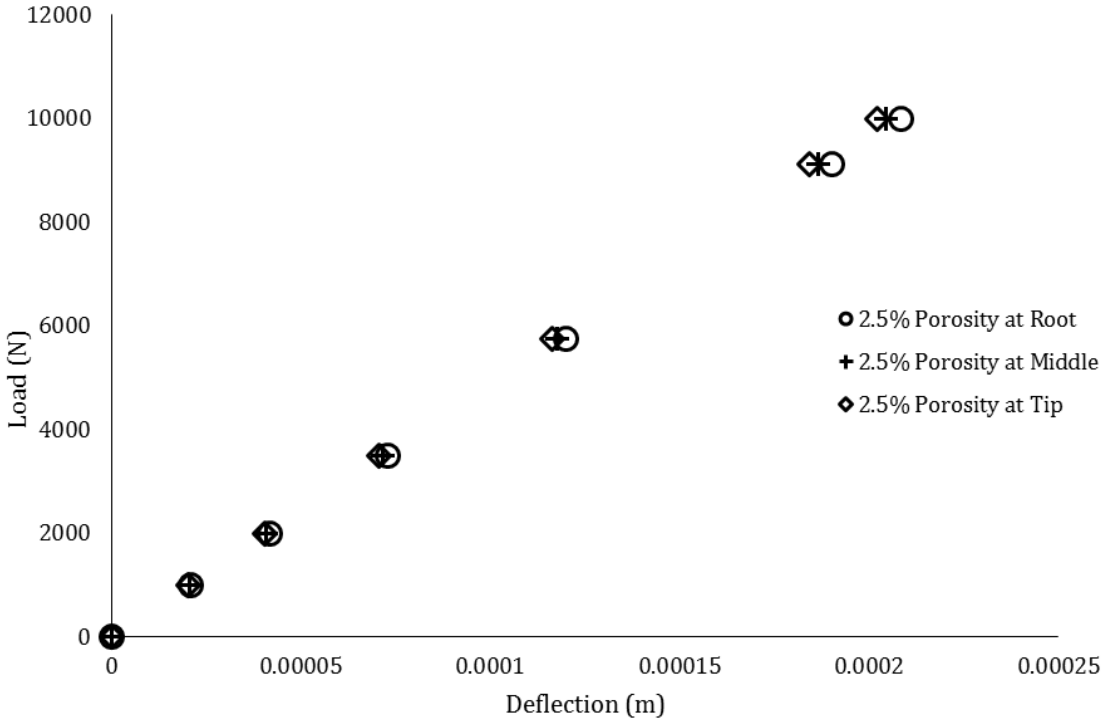

Figure 2-12 - Load-Deflection for 2.5% porosity at various locations along beam length

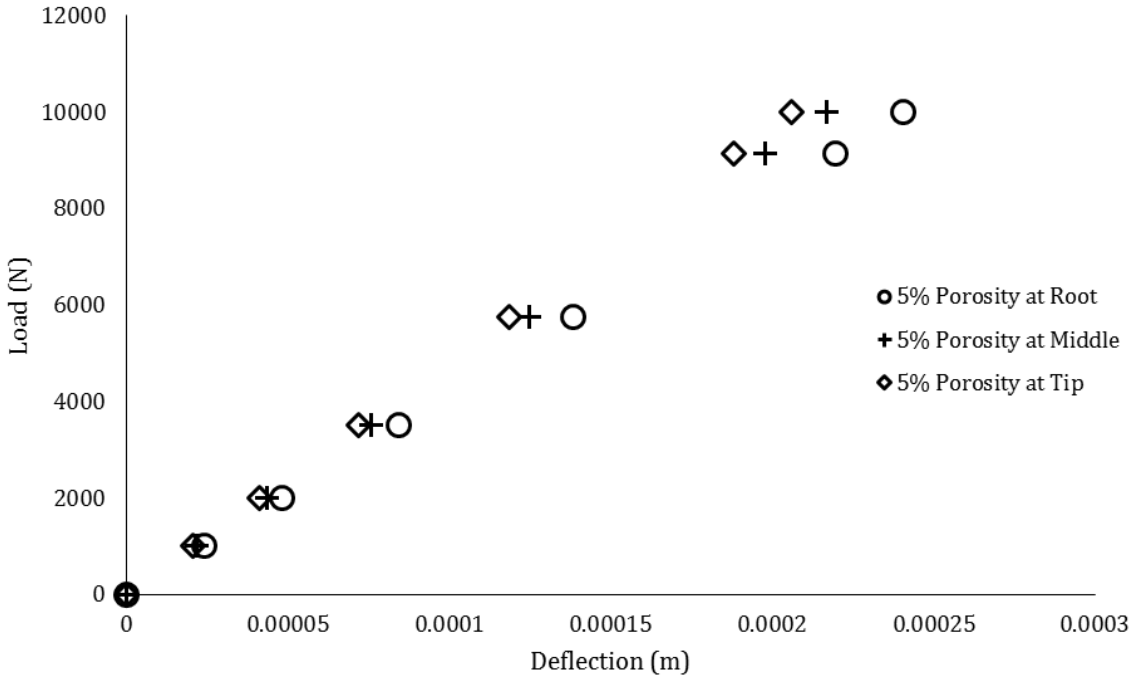

Figure 2-13 - Load-Deflection for 5% porosity at various locations along beam length

Figure 2-14 shows the reduction in elastic modulus due to pore location and total porosity of a cantilever beam undergoing bending due to an applied tip load. Compared to the work of Morrissey and Nakhla [4], which showed pore location and orientation did not influence the reduction in elastic modulus of a plate with a hole undergoing tensile loading, the same cannot be said for a beam undergoing bending. When low porosity beams are placed in bending the pore location clearly influences the percent reduction in elastic modulus. This is expected since the normal stresses vary along the length of the beam. The percent reduction increases significantly as pores are moved closer to the root. For example, at 2.5% total porosity the percent reduction in elastic modulus increases from 1.4% at a point five-sixths of the total length away from the root to 4.0% at one-sixth of the total length away from the root.

Moreover, this increase is even more pronounced for 5% total porosity. At 5% total porosity, the percent reduction increased from 2% at five-sixths of the total length away from the root to 16% at one-sixth of the total length away from the root. As such, it is clearly demonstrated that pore location influences the reduction in elastic modulus, especially at higher porosities, with the largest reduction occuring with porosities concentrated at the root. This result is expected since the normal stresses will reach a maximum at the root for a cantilever undergoing tip loading.

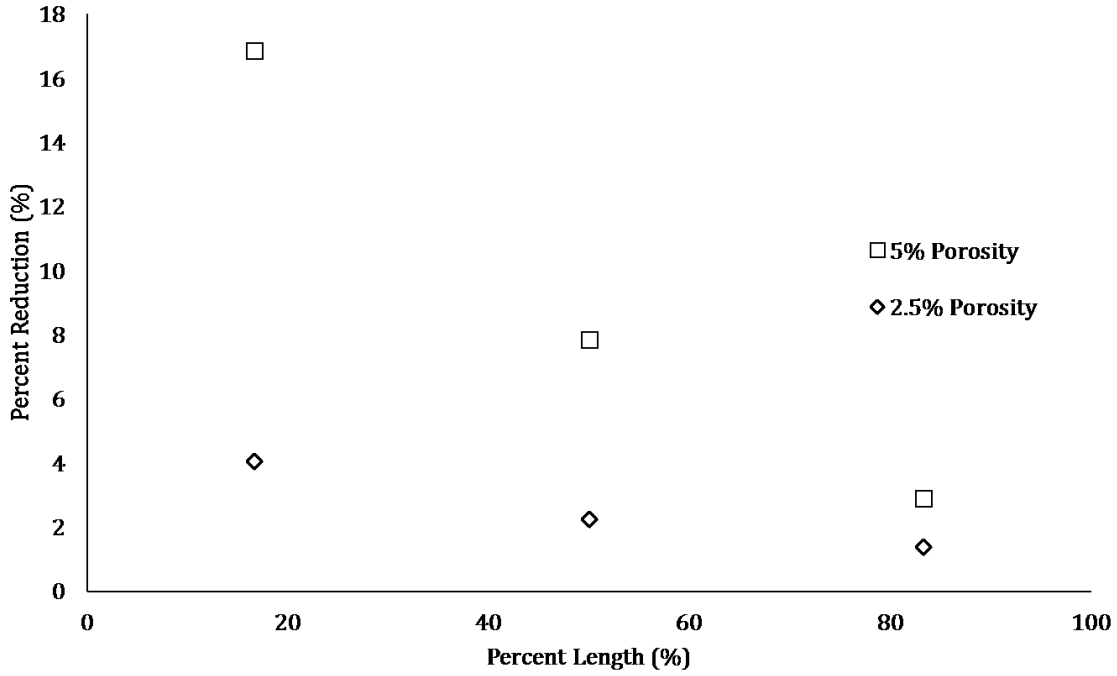

Figure 2-14 - Percent reductions in modulus due to porosity concentration along percent length of the beam.

2.4.3. Finite Element Model – Three-Dimensional Beam

In Figure 2-15, the Abaqus FE models completed for this study are compared with experimental load versus deflection data reported in [5]. The limits of the results to which all other models should be contained within are the experimental results from [5] and the pore free Perfect beam FE model from this study. These limits are

clear since a higher modulus cannot be predicted for a beam with pores than a beam without pores, and a lower modulus cannot be predicted than the experimental data as this would indicate the simulation was not representative of the experiment. From this, it is evident that the FE models studied in this study are within these limits and capture the trend of the experimental results from [5] with an average error of +14.8%, as compared with the calculated approximate error of +38% reported in [5]. It can be observed from Figure 2-15, the FE models for total porosities of 2.5% concentrated in various segments along the beam show that there is a minimal effect to reduce the modulus of the beam. A similar trend is found in the 5% porosity FE models, with the exception of the FE model where the 5% porosity is concentrated at the root. As such, it is evident that unless porosities are concentrated towards the root, the effect on reducing the load-deflection curve is minimal.

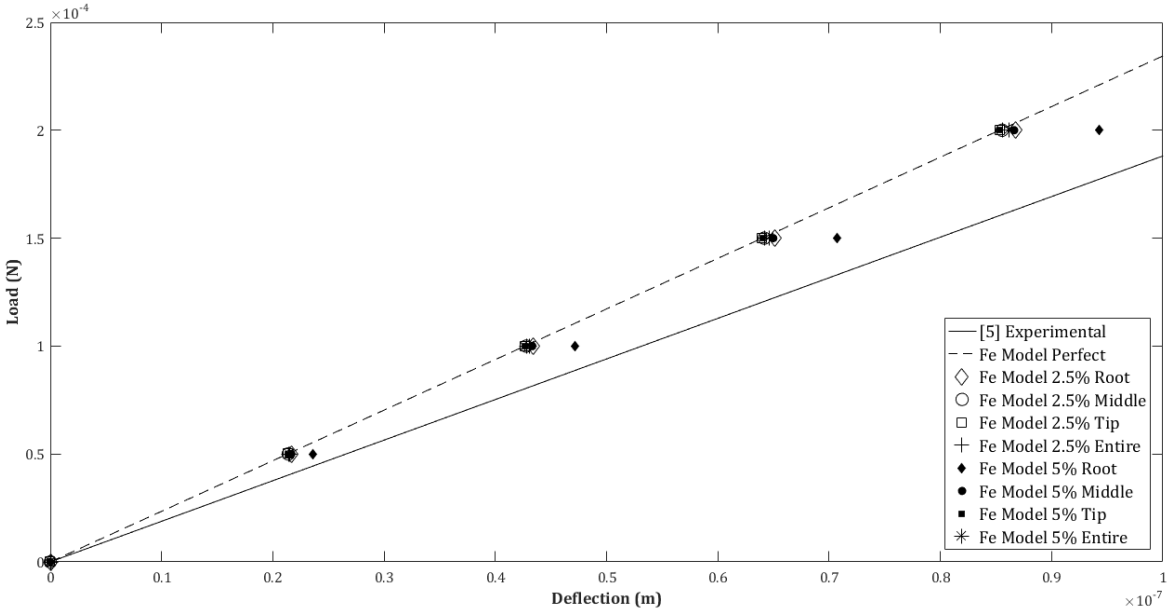

Figure 2-15 - Load-Deflection Comparison of This Study with [5] Experimental.

Some of the error in the FE models can be contributed to the assumptions made in this study. The FE models completed in this study assumed a uniform, constant cross-section, free of imperfections, which is not the case when observing SEM images of the beam in [5]. As well, the FE models were isotropic due to the single-grain assumption, but as reported in [5] this was not true. Lastly, the porosity concentration in the FE models completed in this study do not include the effect of pores away from the neutral plane – it is assumed the porosity is concentrated uniformly across the cross-section with no bias away from the neutral plane. Without more information provided in [5] on the exact location and size of pores it is difficult to model various pore sizes in various locations and obtain accurate results which replicate the experiment. As well, this last assumption may have a large effect on the accuracy of the FE model, since for a cantilever beam undergoing bending due to tip loading, the maximum normal stresses are located at the root, but away from the neutral plane and towards the upper and bottom surfaces. Therefore, if the porosity, especially if it is a singular large pore, is located at the point where normal stress is approaching the maximum, the effect on reducing elastic modulus will be the greatest. The presence of a large pore would also violate the assumption that the cross-section remained constant as a large pore would cause the cross-section to vary along the beam length throughout the pore. As well, if the large pore is located close to the surface of the beam it is probable it would be present as a surface defect or hole, also changing the cross-section along the length. Such defects can be seen in SEM images reported in [5]. Due to the assumptions and the inability to enhance the FE model any further, the authors are satisfied with the accuracy of the model.

Next, a comparison between all FE models by this study and by Gong is made with the experimental data in Figure 2-16. It is first noted that several of Gong's FE models predict a higher modulus than the Perfect beam FE model, which is not possible as previously stated. From Gong's results, it is evident that the Single Pore Root FE model has the largest effect, comparable to this study's FE model for 5% porosity concentrated at the root. This single pore is located approximately in the location of maximum normal stress; however, the exact placement from the neutral plane is unknown and as such it is difficult to compare to the FE models completed in this study. From observing Figure 2-15 and Figure 2-16, it is evident that porosity location does have an effect on the modulus of elasticity of a cantilever.

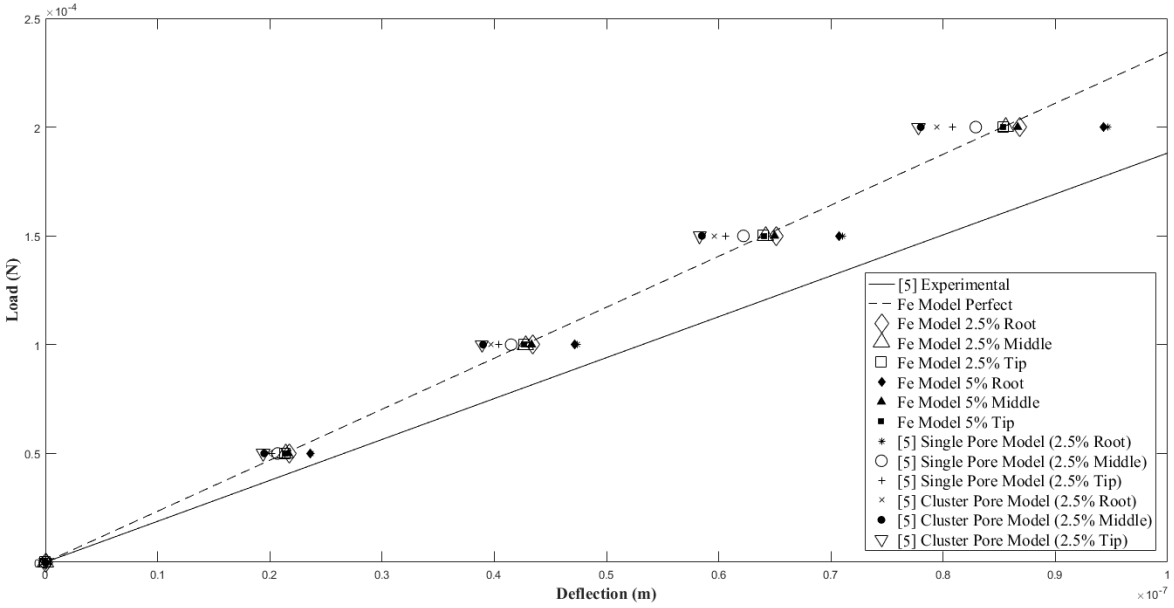

Figure 2-16 - Load-Deflection Comparison of All Data.

A final comparison of porosity uniformly distributed throughout the entire length of the beam to porosity concentrated at various locations is made for 2.5% and 5% porosities in Figure 2-17 and Figure 2-18, respectively.

As can be seen from Figure 2-17 and Figure 2-18, the effect of the location of porosity concentration diminishes if the total porosity is uniformly distributed along the beam or is concentrated beyond half the beam length. This is intuitive since, if the porosity is concentrated in a region of lesser stress – away from the root – its effect to reduce modulus is less pronounced. Similarly, if the same porosity concentration is distributed over the entire length there is less "total" porosity in each segment. In other words, 2.5% total porosity distributed evenly results in approximately 0.8% total porosity in each segment (root, middle, and tip); thus, resulting in less porosity in a region of higher stresses. Comparatively, 5% total porosity distributed over the entire length results in approximately 1.7% porosity in each beam segment. Since this value is less than 2.5%, which showed to have minimal effect on reducing the modulus even when concentrated at the root, the 5% total porosity distributed over the beam length will also have minimal effect on reducing the modulus.

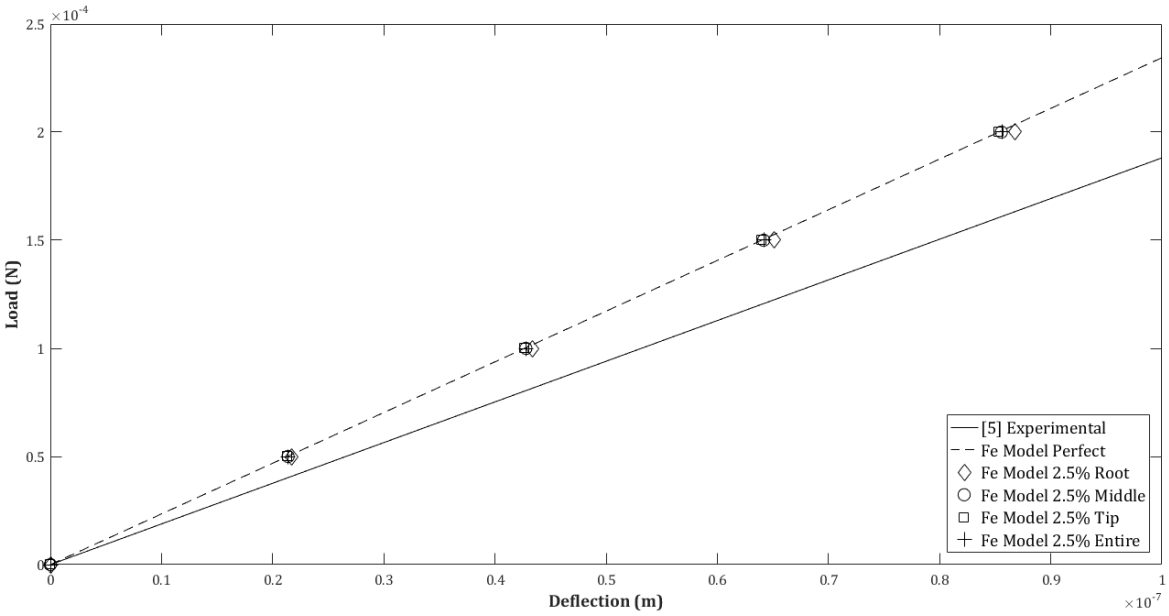

Figure 2-17 - Load-Deflection Comparison for 2.5% Porosity

The FE models completed in this study, which assume uniform porosity distribution across the cross-section throughout various segments of the beam, have shown with certainty that porosities of 5% have a large effect on the behavior of the beam when concentrated close to the root. However, if these large porosities are uniformly distributed over the length, or concentrated in a location away from the root – at or beyond half the beam length – the effect decreases drastically. As for porosities of 2.5% and lower, it can be concluded that there is minimal effect on the beam's modulus regardless of distribution and concentration throughout the length.

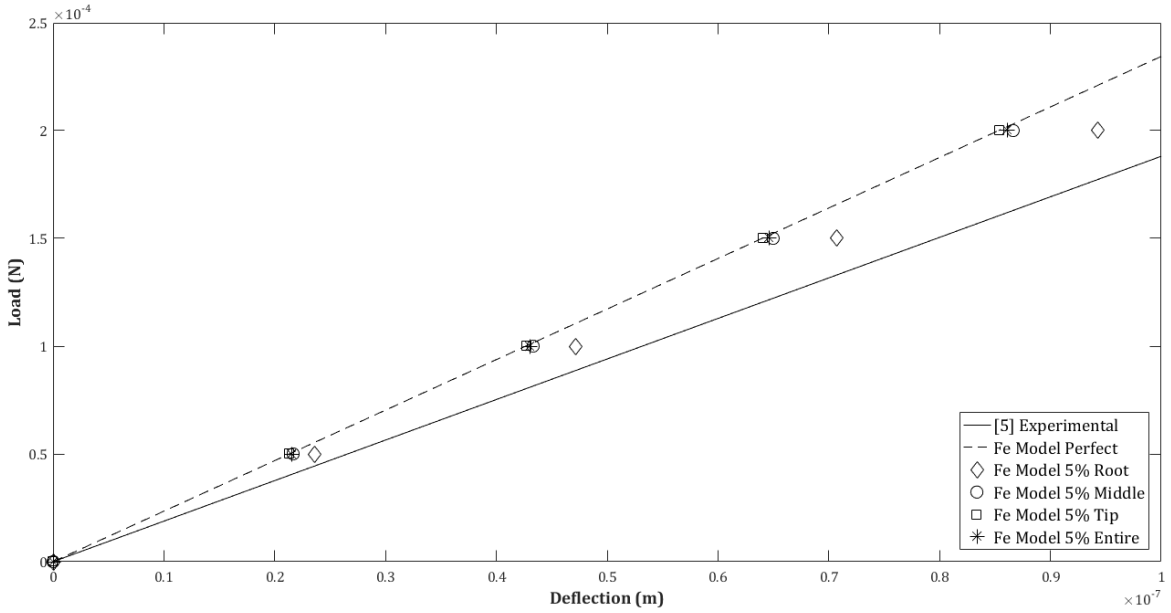

Figure 2-18 - Load-Deflection Comparison for 5% Porosity

2.5. Conclusions

This study supports the results from Morrissey and Nakhla [4] – a macroscale FE model is able to capture the effect of a microscale property such as microporosity on elastic modulus. This study has also proven that to perform the analysis of microcantilevers effectively and accurately, one should utilize Timoshenko beam

theory paired with a 3D FE model. This is because Timoshenko beam theory works with various slenderness ratios and 3D FE model can capture Poisson's effect, can model non-ideal boundary conditions, and provides realistic modelling of the analysis. Lastly, this study has proven that the amount of porosity and the location of porosity concentration have a clear effect on the elastic modulus. Several cases were analyzed and it was determined that porosities concentrated at the root have the largest effect on the elastic modulus of a cantilever, while porosities uniformly distributed over the length, or concentrated away from the root, have minimal effect on elastic modulus.

Acknowledgements

The authors are grateful for the financial support from Suncor Inc.

References

1. N. I. Romanova, G. S. Kreimer, and V. I. Tumanov, "Effects of residual porosity on the properties of tungsten carbide-cobalt hard alloys," Soviet Powder Metall Met Ceram, vol. 13, pp. 670-673, August 1974.
2. R. A. Hardin and C. Beckermann, "Effect of porosity on the stiffness of cast steel," Metall and Mat Trans A, vol. 38, pp. 2992-3006, December 2007.
3. L.S. Morrissey, S. Handrigan, and S. Nakhla, "Quantifying void formation and changes to microstructure during hydrogen charging: a precursor to embrittlement and blistering," Metall and Mat Trans A, in press, doi: 10.1007/s11661-018-5071-8
4. L. S. Morrissey and S. Nakhla, "A finite element model to predict the effect of porosity on elastic modulus in low porosity materials," Metall and Mat Trans A, vol. 40, pp.2622-2630, July 2018.
5. B. Gong, Finite Element Analysis of Micro-Cantilever Beam Experiments in UO2, November 2015.
6. D. Di Maio and S. G. Roberts, "Measuring fracture toughness of coatings using focused-ion-beam-machined microbeams," Mat Res, vol. 20, pp. 299-302, February 2005.

7. K. Gofryk et al., “Anisotropic thermal conductivity in uranium dioxide,” Nat. Commun., August 2014.
8. F. Gupta, A. Pasturel, and G. Brillant, “Diffusion of oxygen in uranium dioxide: A first-principles investigation,” Ohys. Rev. B, vol. 81, January 2010.
9. M. Asmani, C. Kermel, A. Leriche, and M. Ourak, “Influence of porosity on young’s modulus and poisson’s ratio in alumina ceramics,” Euro Cera Soci, vol. 21, pp. 1081-1086, August 2001.
10. C. Yu, S. Ji, and Q. Li, “Effects of porosity on seismic velocities, elastic moduli and poisson’s ratios of soli materials and rocks,” Rock Mech and Geotech Eng, vol. 8, pp. 35-49, February 2016.
11. Gibson LJ, Ashby MF. Cellular solids, 2nd ed. Oxford: Pergamon Press; 1997
12. D. R. Olander, Fundamental Aspects of Nuclear Reactor Fuel Elements, p. 335, 1976.

3. Chapter 3: A Molecular Dynamics Analysis of Atomistic-scale Vacancies in various metals to predict the Reduction in Elastic Modulus

Abstract: The effect of vacancy percentage is tested to predict reduction in elastic modulus. Two materials are tested – pure iron and iron-chromium. Several force fields and parameter sets are compared using molecular dynamics simulation. Comparisons to experimental data and Finite Element model from literature are made. It is determined that molecular dynamics simulations captures trend of reducing elastic modulus due to vacancy percentage.

3.1. Introduction

With the increased viability of computer-based simulations, Morrissey and Nakhla [1] have demonstrated that the effect of a microscale property (porosity) on the strength of a material can be captured using a macroscale Finite Element (FE) model. Morrissey and Nakhla [1] built a FE model to perform uniaxial tension on a slab of material with a hole, where the size of the hole was dependent on a percentage of porosity ranging from 0 to 10%. For each value of porosity, a value for the reduction in modulus was determined. Their FE model had an average error of less than 1% compared to experimental data from literature.

In addition, the work of Handrigan et al. demonstrated the capabilities of a macroscale FE model to capture the effect of a microscale property (porosity) on the elastic modulus and behavior of a cantilever [2]. The work of Handrigan et al. built upon the original work of Morrissey and Nakhla [1] to allow for accurate analysis and determination of the load-deflection curve and calculation of elastic modulus for a microcantilever beam. Using the experimental data provided in [3], Handrigan et al. developed a FE model which replicated the experimental setup without performing the experiment themselves. In [3], microcantilevers were created in a slab of Uranium Oxide and then put under bending until failure through the application of a tip load created by a nanoindenter. An experiment of this type has high associated costs, not only with equipment CAPEX, but also through sample preparation and experimentation. With limited information on sample geometry, grain orientation, and imperfections, Handrigan et al. were able to capture the trend of experimental

results with an average error of +14% – compared to the average error of +38% calculated from [3].

Since the effect of porosity, a microscale property, could be captured through the application of macroscale FE models, it is now postulated that the effect of porosity can be captured on the atomistic-scale using molecular dynamics simulations.

Building upon the work of Morrissey and Nakhla [1], this work will attempt a similar procedure except on the atomistic-scale using molecular dynamics. On the atomistic-scale, the percentage of vacancies will be thought of as porosity percentage (i.e., 1% porosity corresponds to 1% vacancies) since porosity is essentially a void of material within a body.

To perform accurate atomistic simulations, an accurate force field and parameter set is required. The work of Rajabpour et al. [4] first demonstrated how the chosen force field affected the determination of elastic constants of an iron and iron-carbon system, clearly demonstrating the accuracy of several force fields. Expanding upon this work, the work of Morrissey et al. [5] tested various types of force fields, such as Embedded Atom Method (EAM), Modified Embedded Atom Method (MEAM), Tersoff, and ReaxFF, each with various parameter sets, to test the applicability of different force fields to replicate a macroscale uniaxial tension test through atomistic modelling. It was concluded that ReaxFF was on average the most accurate for obtaining an accurate elastic modulus for pure iron.

3.2. Molecular Dynamics

Molecular Dynamics involves the simulation of atom and molecule movement. With known position and velocity of the atoms, Newton's equations of motion are applied to predict future positions and velocities relative to the acceleration of each atom. This acceleration is formulated from the interaction of particles through the use of a force field which provides information regarding the interaction between certain atom types. From this acceleration, the positions and velocities are updated step-by-step until the simulation has finished.

In this study, several types of force fields, with various parameter sets for each, are investigated. These include EAM, MEAM, Tersoff, and ReaxFF.

3.2.1. Embedded Atom Method (EAM)

Based upon the quasiatom theory, Daw and Baskes proposed the EAM force field to avoid the problem of defining an accurate volume [6]. Daw and Baskes avoided volume-dependency by using the electron embedding energy, a property dependent on electron-density, since the density of a system is always definable. Daw and Baskes stated that the EAM force field increases the accuracy of elastic properties of solids compared to previous pair-potential methods since these pair-potentials depended upon the volume-dependent energy whereas the EAM did not. The total energy in the EAM is defined in equation (3-1):

$$E_{tot,EAM} = \sum_{i} F_i(\rho_{h,i}) + \frac{1}{2}\sum_{\substack{i,j \\ i \neq j}} \phi_{ij}(r_{ij}) \tag{3-1}$$

where, $\rho_{h,i}$ is the host electron density at atom *i* due to the remaining atoms in the system, $F_i(\rho)$ is the energy to embed atom *i* into the background electron density ρ, and $\phi_{ij}(R_{ij})$ is the core-core pair repulsion between atoms *i* and *j* separated by the distance R_{ij}. By summing over many atoms of the system, EAM is considered a multibody potential. More detail on the EAM force field can be found in [6].

3.2.2. Modified Embedded Atom Method (MEAM)

Lee et al. built upon the original EAM force field to develop the MEAM force field through the addition of angular forces. Lee et al. proposed the applicability of the EAM potential to include Face-Centered Cubic (FCC), Body-Centered Cubic (BCC), and Hexagonal Close-Packed (HCP) crystal structures for metals and alloys could be possible through the inclusion of angular forces [7]. The total energy in the MEAM force field is defined in equation (3-2):

$$E_{tot,MEAM} = \sum_i \left\{ F_i(p_i) + \frac{1}{2}\sum_{i \neq j} \phi_{ij}(R_{ij}) \right\} \tag{3-2}$$

where *F* is the embedding energy term which is a function of atomic electron density (p_i), ϕ_{ij} is the core-core pair repulsion between atoms *i* and *j* separated by distance R_{ij}. Similar to EAM, the summation over many atoms within the system allows the MEAM force field to also be considered a multibody potential. More detail on the MEAM force field can be found in [7].

3.2.3. Tersoff

The Tersoff force field was developed to avoid the increased number of free parameters as are present in the multibody force fields of EAM and MEAM. Through

avoiding the general N-body form, the Tersoff potential is both tractable and accurate since it was developed around real system physics [8].

The Tersoff potential is bond order dependent. Bond order for each atom depends upon the neighbouring atoms and is highly influential to the physics of the system. While it is believe that an atom with many neighbours is said to form weaker bonds than atoms with few neighbours, Tersoff stated the most important factor to be determined is the coordination number. The coordination number is said to be the number of neighbouring atoms close enough to form bonds [8]. The total energy in the Tersoff force field is defined in equation (3-3), with a detailed explanation of variables provided in [8]. More detail on the Tersoff force field can be found in [8].

$$
\begin{aligned}
E &= \frac{1}{2}\sum_{\substack{i,j \\ (j\neq i)}} V_{ij} \\
V_{ij} &= f_C(r_{ij})\left[f_R(r_{ij}) + b_{ij} f_A(r_{ij})\right] \\
f_C(r) &= \begin{cases} 1 & if\ r < R - D \\ \frac{1}{2} - \frac{1}{2}\sin\left(\frac{\pi}{2}\frac{r-R}{D}\right) & R - D < r < R + D \\ 0 & r > R + D \end{cases} \\
f_R(r) &= Aexp(-\lambda_1 r) \\
f_A(r) &= -Bexp(-\lambda_2 r) \\
b_{ij} &= (1 + \beta^n {\zeta_{ij}}^n)^{-\frac{1}{2n}} \\
\zeta_{ij} &= \sum_{k\neq i,j} f_C(r_{ik}) g(\theta_{ijk}) \exp[{\lambda_3}^m (r_{ij} - r_{ik})^m \\
g(\theta) &= \gamma_{ijk}\left(1 + \frac{c^2}{d^2} - \frac{c^2}{[d^2 + (cos\theta - cos\theta_0)^2]}\right)
\end{aligned}
\tag{3-3}
$$

3.2.4. Reactive Force Field (ReaxFF)

Originally proposed by van Duin et al. [9], the ReaxFF force field is a bond order dependent force field, similar to the Tersoff force field. The inclusion of bond order allows for contributions due to various bonding (sigma, pi, and double-pi) over the distance between atoms. In addition to bond order inclusion, the added benefit of the ReaxFF force is the ability to simulate dynamic formation and breaking of bonds within the system. The energy defined in the ReaxFF force field is shown in equation (3-4), while the equation of bond order is shown in equation (3-5). More detail on the ReaxFF force field can be found in van Duin et al. [9].

$$E_{system} = E_{bond} + E_{over} + E_{under} + E_{lp} + E_{val} + E_{tor} + E_{vdWaals} + E_{Coulomb} \quad (3\text{-}4)$$

$$BO_{ij}{}^{i} = BO_{ij}{}^{\sigma} + BO_{ij}{}^{\pi} + BO_{ij}{}^{\pi\pi} \quad (3\text{-}5)$$

3.3. Methodology

Similar to the work of Morrissey et al. [5], this work tests the effectiveness of various force fields and parameter sets to predict the elastic modulus of iron, but extends the work to predict the reduction in elastic modulus due to the presence of vacancies. To perform this work, a BCC body of pure iron atoms was placed in tension at room temperature to replicate a macroscale uniaxial tension test. From this, the stress-strain curves were generated and analyzed to determine the mechanical properties. Comparisons were made to Morrissey et al. to ensure zero vacancy

systems were accurate to previous work. Afterwards, the study on the effect of vacancies was performed for both pure iron and iron-chromium. Molecular dynamics simulations were carried out using Large-scale Atomic/Molecular Massively Parallel Simulator (LAMMPS), as developed by Sandia National Laboratories [10].

First, a unit cell of pure iron was created and replicated to obtain 2000 total atoms with zero vacancies in a 28.5 Å x 28.5 Å x 28.5 Å cube with periodic boundary conditions. Next, from this block of pure iron atoms, atoms were selected at random and removed to create vacancies ranging from 1 to 10%. As was concluded in [5], in general, the ReaxFF force field is most accurate for a uniaxial tension test; however, a study on the various force fields is required to test whether or not another force field is more accurate for predicting the reduction of elastic modulus due to vacancy percentage.

Unfortunately, outside of certain laboratory experiments, the use of pure iron is not common, as in its pure state, iron does not have favourable properties. As such, a study on a stainless steel would be more worthwhile; however, due to the limitation of available parameter sets for the various force fields, this is not feasible. Therefore, iron with 13% chromium is studied using the two available parameter sets which include iron-chromium bonds. While several parameter sets exist for the ReaxFF force field, only one includes iron-chromium bond definitions, as such only this parameter set can be tested for ReaxFF. The other parameter set to be tested for iron-chromium is for the EAM force field.

For the iron-chromium system, the block of pure iron containing 2000 atoms from before was then turned into iron-chromium by selecting, at random, 13% of the iron atoms and substituting them for chromium atoms to obtain a block of iron-chromium. Similar to how vacancies were created for the pure iron, vacancies were created in the iron-chromium system.

Following a similar procedure outlined by Morrissey et al. [5], the input parameters for each force field were determined and can be seen in Table 3-1.

Table 3-1 - Molecular Dynamics Parameters

Parameter	EAM	MEAM	Tersoff	ReaxFF
Temperature	300K	300K	300K	300K
Time step	0.001 ps	0.001 ps	0.001 ps	0.25 fs
Equilibration	50 ps	50 ps	50 ps	50 ps

Each system was equilibrated for 50 ps at 300K using a dynamic Nose-Hoover NPT barostat. The systems were allowed to adjust the lattice under natural expansion and contraction throughout the equilibration process. As a rough guideline, pressure and temperature were damped using coefficients equal to 1000 and 100 times the time step for each force field, respectively.

Once the system was equilibrated, it was then deformed in one direction under NPT at 300K with zero pressure to allow for natural Poisson contractions in the transverse directions. To ensure only the linear elastic region of the stress-strain curve is obtained, strains are kept to a maximum of 2%, thus allowing for the use of

Hooke's law. The 2% strain was applied over 2 ps for each system, which meant adjusting time steps and strain rates for each individual force field. It was shown in [11] that the time step and strain rate have minimal affect over the linear region of the stress-strain curve, as such the authors are comfortable with adjusting both parameters to ensure each system is strained to 2% over 2 ps of simulation time.

3.4. Results

Since a study on the accuracy of force field and parameter set on predicting the elastic modulus of a pure iron system was performed in Morrissey et al. [5], the results for this study will touch briefly on the modulus calculated at 0% vacancy but will focus on comparing the reduction in modulus as vacancies increase.

First, as can be seen in Table 3-2, the values obtained for the 0% vacancy simulations of pure iron in this study are compared to the work of Morrissey et al. [5]. The values show favorable agreement between the two studies. This study further tested additional ReaxFF parameter sets due to the inclusion of Chromium atoms, the results of which are also included in Table 3-2. Unfortunately, only one of the additional parameter sets include iron-chromium bonds and cannot be compared to an iron-chromium system. As it can be seen, several of the parameter sets for the various force fields are not able to predict the nominal modulus of 200 GPa for iron [12-15] within a small margin of error (<10%). The EAM and MEAM force fields are, on average, highly inaccurate in predicting elastic modulus, with errors as high as 54%. Conversely, the Tersoff and ReaxFF parameter sets, on average, predict the elastic modulus of iron with less error. The authors must state that the accuracy of

any parameter set, regardless of the type of force field, is highly dependent on how it was parameterized. Several of the parameter sets studied were not exclusively developed for predicting mechanical properties. As such, care must be taken when using parameter sets to ensure they are parameterized to calculate the desired properties. Regardless, this study was performed on several of the currently available parameter sets to determine their applicability for predicting elastic modulus.

Table 3-2 - Comparison of Predicted Elastic Modulus

Force Field	Parameter Set	Elastic Modulus (GPa) (This study)	Error from Nominal	Elastic Modulus (GPa) [5]	Error from Nominal	Ref.
EAM	MCM2011	171.95	-14.0%	172	-14.0%	[16]
	Fe_mm	141.5	-29.3%	141.5	-29.3%	[17]
	Mishin2006	129.65	-35.2%	129	-35.5%	[18]
	Average	**147.7**	**-26.2%**	**147.5**	**-26.3%**	-
MEAM	Asadi	92.8	-53.6%	93	-53.5%	[19]
	Etesami	116.4	-41.8%	116.4	-41.8%	[20]
	Average	**104.6**	**-47.7%**	**104.7**	**-47.7%**	-
Tersoff	FeC_Henriksson	218.7	9.4%	218	9.0%	[21]
	Average	**218.7**	**9.4%**	**218**	**9.0%**	-
ReaxFF	CHOFe	137.6	-31.2%	-		[22]
	FeOCHCl	182.4	-8.8%	182	-9.0%	[23]
	CHOFeAlNiCuS	164.8	-17.6%	165	-17.5%	[24]
	CHOFeAlNiCuSCr	164.5	-17.8%	-		[25]
	CHOFeAlNiCuSCr_v2	164.4	-17.8%	-		[26]
	CHOFeAlNiCuSCr_v3	165	-17.5%	-		[27]
	CHOFeAlNiCuSCrSiGe	164.6	-17.7%	-		[28]
	Average	**163.3**	**-18.3%**	**173.5**	**-13.3%**	-

For an in-depth description of the parameterization for each parameter set, see Table 3-2 for the respective reference. In general, force fields are parameterized using various values calculated from quantum mechanics, while some include parameterization with the values of the elastic constants. In general, elastic constants

are determined through analysis of wide range frequency responses of electrical impedance within the crystal [29], which is not directly related to the elastic modulus. As such, while parameter sets parameterized with the elastic constants are accurate for predicting the elastic constants, they are inaccurate for predicting the elastic modulus during a uniaxial tension test. To obtain a parameter set capable of predicting an accurate elastic modulus from an atomistic uniaxial tension test, parameterization with the elastic modulus should be performed.

As can be seen prior, the individual parameterization of each parameter set highly influences the prediction of elastic modulus, regardless of force field. When comparing the three EAM parameter sets, neither can predict an accurate modulus and the values predicted between the three parameter sets are largely varied. Similarly, both MEAM parameter sets tested were unable to predict an accurate modulus, but predicted an elastic modulus closer in value.

As discussed previously in this work, and in [5], many of the parameter sets were not intended for the prediction of elastic modulus. Of key importance are the ReaxFF parameter sets. The ReaxFF parameter sets tested have not included parameterization with the elastic constants and are, on average, the most accurate for predicting the elastic modulus. The authors believe that the inclusion of bond order in ReaxFF allows for more accurate prediction of elastic modulus. This is also evident in the single Tersoff parameter set which is also bond order dependent.

Next, a comparison of the percent reduction in modulus versus the percent vacancy is shown in Figure 3-1. As it can be seen, in general, as vacancies reach and

exceed 5% the accuracy in prediction of the reduction of elastic modulus varies erratically and unpredictably, with some force fields not being as affected as others, depending on the parameter set. For example, two of the three parameter sets for the EAM force field (Mishin2006 and Fe_mm) have erratic values after 6% for Mishin2006 and after 8% for Fe_mm. The third EAM parameter set (MCM2011) has some fluctuation at lower percentages (1-3%), but afterwards is consistent throughout the remaining tested vacancies. As for the parameter sets for the MEAM force field, both exhibit a constant decline in reduction of modulus after 5% vacancies which is unintuitive. Conversely, both Tersoff and ReaxFF force fields appear to be, on average, more capable of dealing with the increase of vacancies with less fluctuations as vacancy percentage increases. This is evident in the single Tersoff parameter set; providing consistent results for all vacancy percentages tested. As for the parameter sets for ReaxFF, all appear to be consistent to about 5-8% vacancies, with large fluctuations appearing after 8% vacancies.

There are several possible reasons for the inaccuracies. The authors believe that at vacancy percentages above 5% it is likely that the vacancies are interacting as the body is deformed, thus influencing the strength of the material. In addition, for Tersoff and ReaxFF, force fields which are bond order dependent, the authors believe that these force fields are, in general, more capable of dealing with increased vacancy percentages due to the inclusion of the bond order since the distance between atoms is not consistent due to presence of vacancies. Lastly, it is possible that the increased number of vacancies is negatively influencing the equilibration of the system. Due to

the erratic behavior after 5% vacancies, the authors have chosen to only study vacancies up until 5% for all force fields.

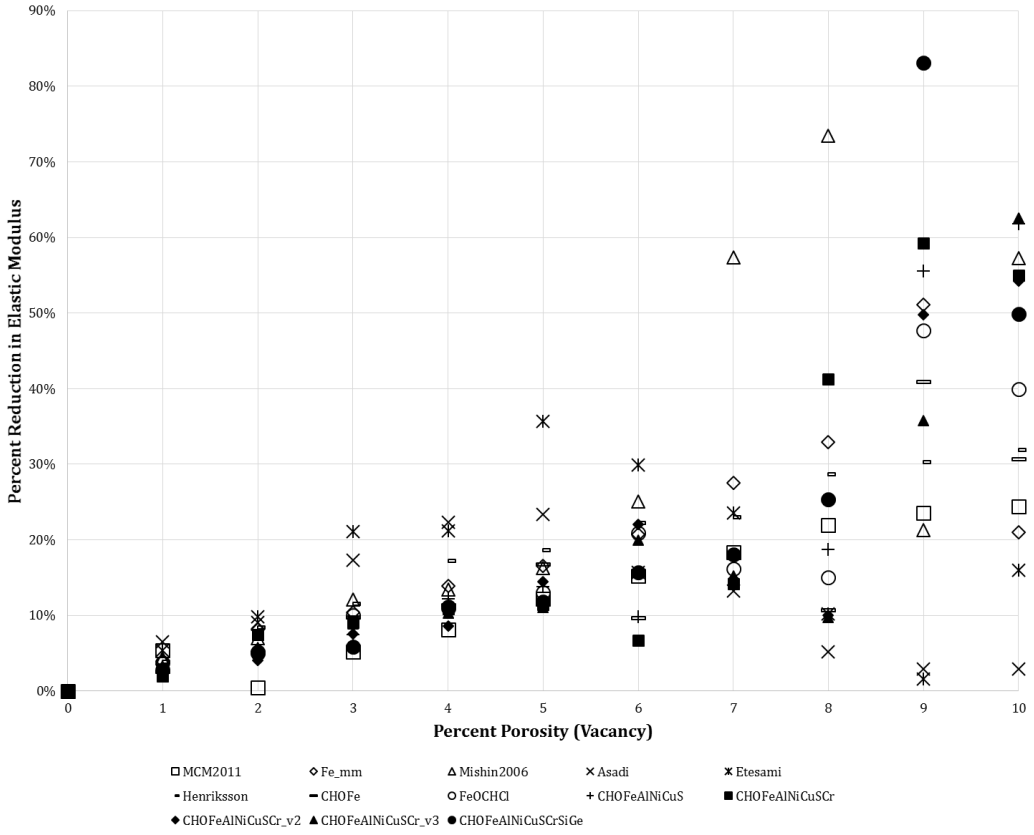

Figure 3-1 - Reduction in Elastic Modulus versus Percent Porosity (Vacancy)

Prior to continuing, the authors must confirm the simulations for zero vacancies until 5% vacancies were run accurately. To confirm the simulations were run as accurately as possible, each system was tested with an NVE ensemble to ensure that energy is conserved within the system. As well, the authors performed an equilibration time sensitivity analysis to verify that each system was adequately equilibrated. Figure 3-2 shows the total energy for each force field over time for one of the simulations, while Figure 3-3 shows the equilibration time versus temperature

for an EAM, MEAM, Tersoff, and ReaxFF simulation. As can be seen from Figure 3-2, the total energy of each system is conserved, thus providing confidence in the results of the simulations. In addition, from Figure 3-3, it is evident that each force field has reach equilibrium well before 50 ps. Since total energy was conserved and the systems reached equilibration well before the deformation, the authors are confident the simulations have been performed as accurately as possible. With confidence the simulations were completed accurately, a discussion on the values for the reduction of elastic modulus due to vacancies is possible.

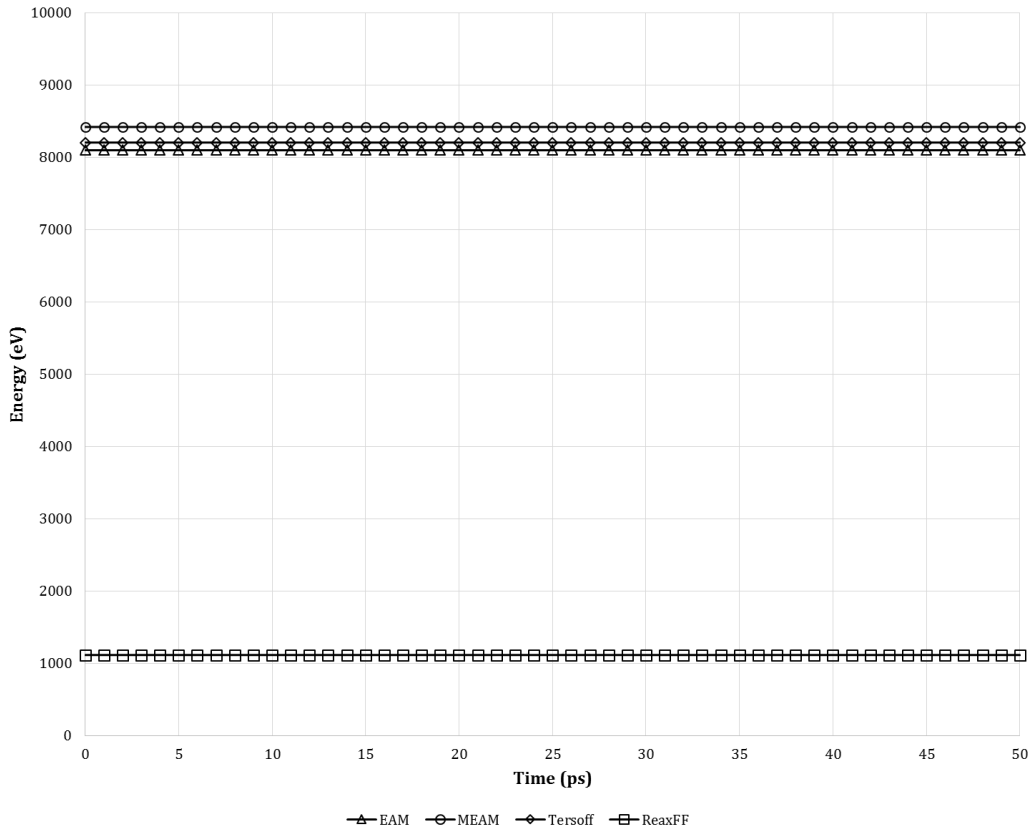

Figure 3-2 - Energy Conservation Check for each Force Field

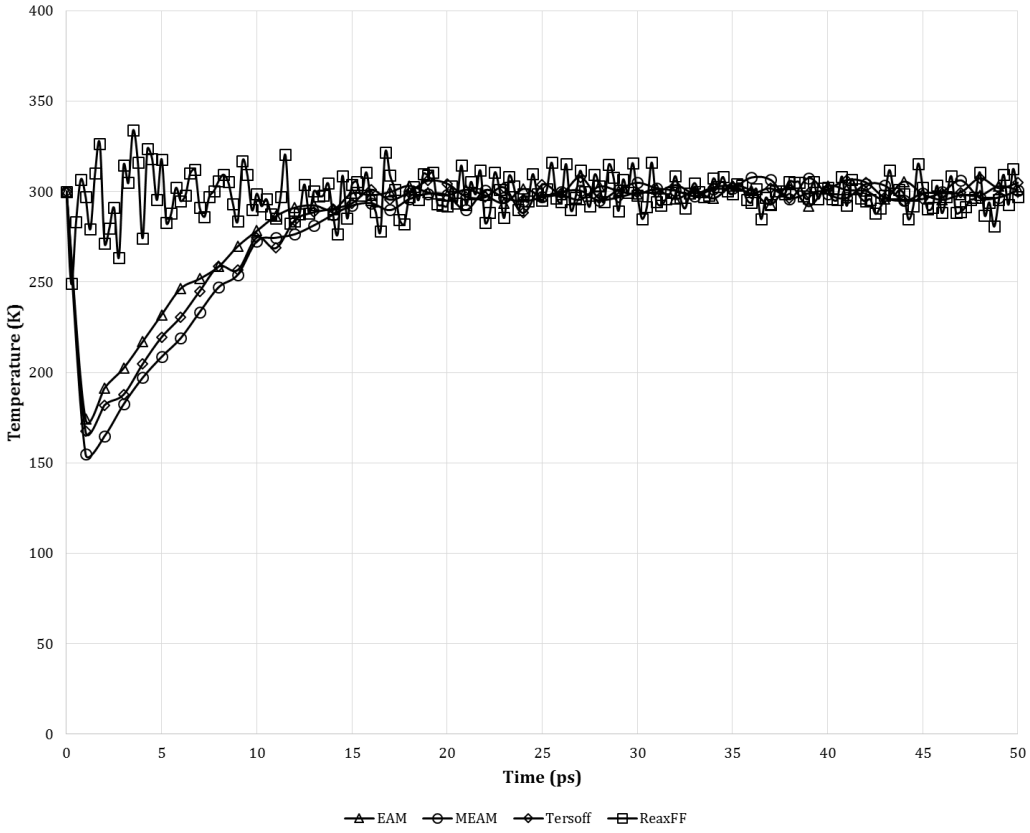

Figure 3-3 - Equilibration Check for each Force Field

While some force fields show inaccurate prediction of modulus and erratic reductions in modulus due to porosity, several others more accurately predict elastic modulus and are more consistent in the predicted reduction in modulus due to porosity to much higher values of porosity (up to 8-9%). It is noted that the parameter sets which predict a more accurate elastic modulus from Table 3-2 are the parameter sets which more accurately predict the reduction in modulus due to vacancy percentage.

The results from the EAM, MEAM, Tersoff, and ReaxFF force fields and their respective parameter sets can be seen in Figure 3-4 to Figure 3-7. Included in each

figure are experimental results of reduction in elastic modulus versus percent porosity and Morrissey and Nakhla's [1] FE model which was developed to predict this reduction. As can be seen in each respective figure, the atomistic model using molecular dynamics simulations and percent vacancies is able to accurately predict the reduction in elastic modulus due to vacancy percent.

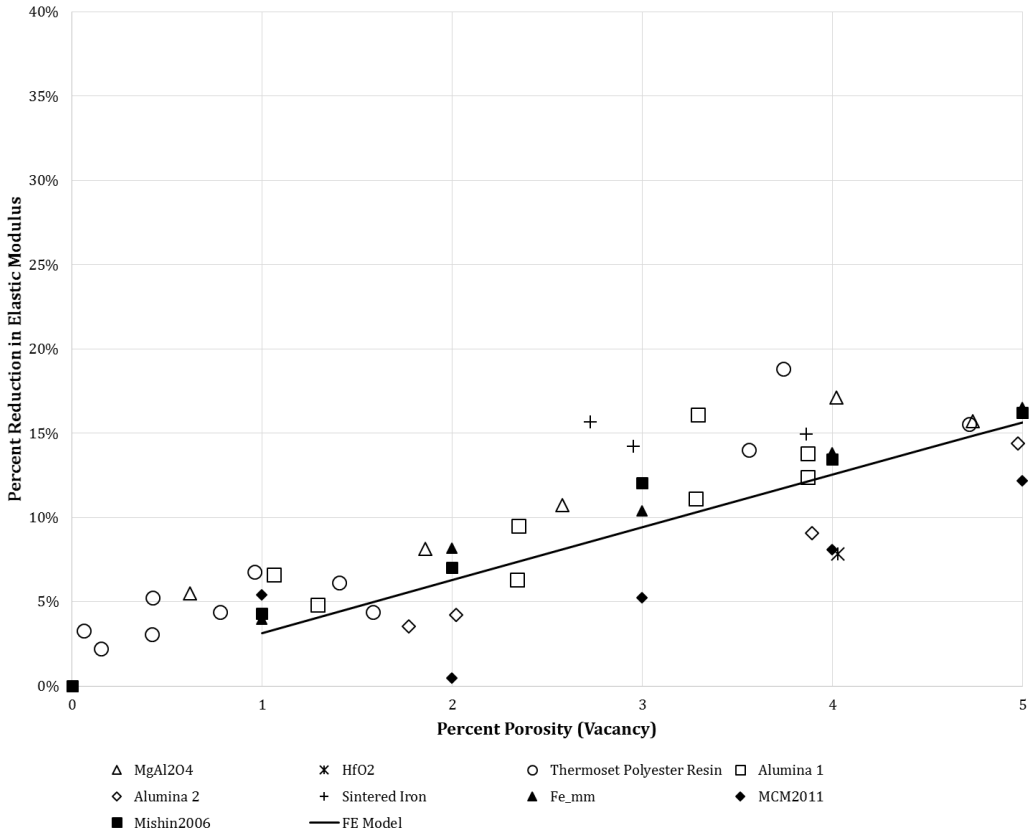

Figure 3-4 - Comparison of EAM for Pure Iron, Morrissey and Nakhla FE Model [1], and Experimental data ($MgAl_2O_4$ [30], HfO_2 [31], Thermoset Polyester Resin [32], Alumina 1 [33], Alumina 2 [34], and Sintered Iron [35]) for the Reduction in Elastic Modulus versus Percent Porosity (Vacancy)

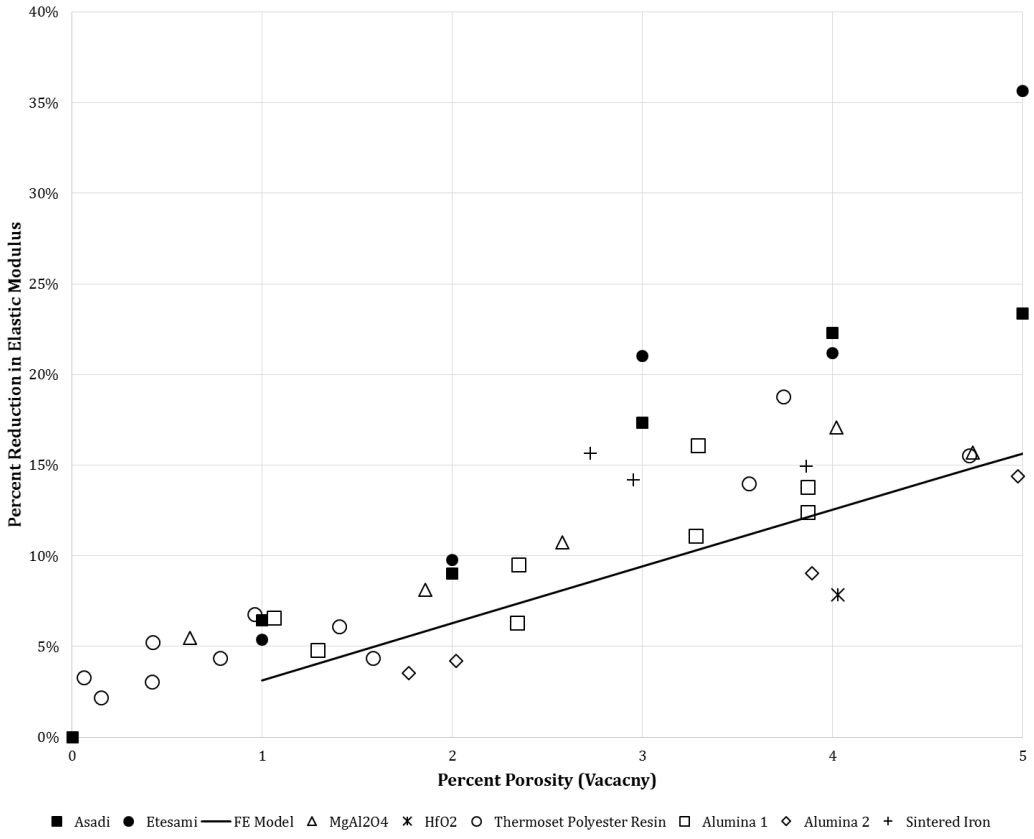

Figure 3-5 - Comparison of MEAM for Pure Iron, Morrissey and Nakhla FE Model [1], and Experimental data ($MgAl_2O_4$ [30], HfO_2 [31], Thermoset Polyester Resin [32], Alumina 1 [33], Alumina 2 [34], and Sintered Iron [35]) for the Reduction in Elastic Modulus versus Percent Porosity (Vacancy)

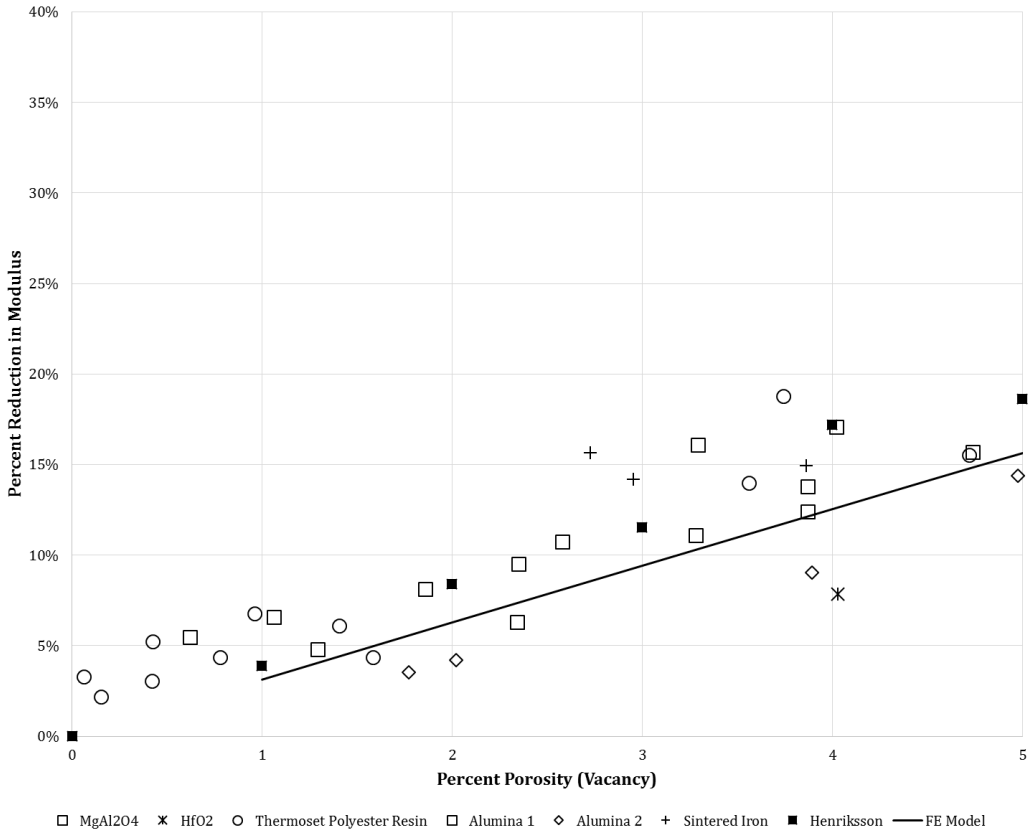

Figure 3-6 - Comparison of Tersoff for Pure Iron, Morrissey and Nakhla FE Model [1], and Experimental data ($MgAl_2O_4$ [30], HfO_2 [31], Thermoset Polyester Resin [32], Alumina 1 [33], Alumina 2 [34], and Sintered Iron [35]) for the Reduction in Elastic Modulus versus Percent Porosity (Vacancy)

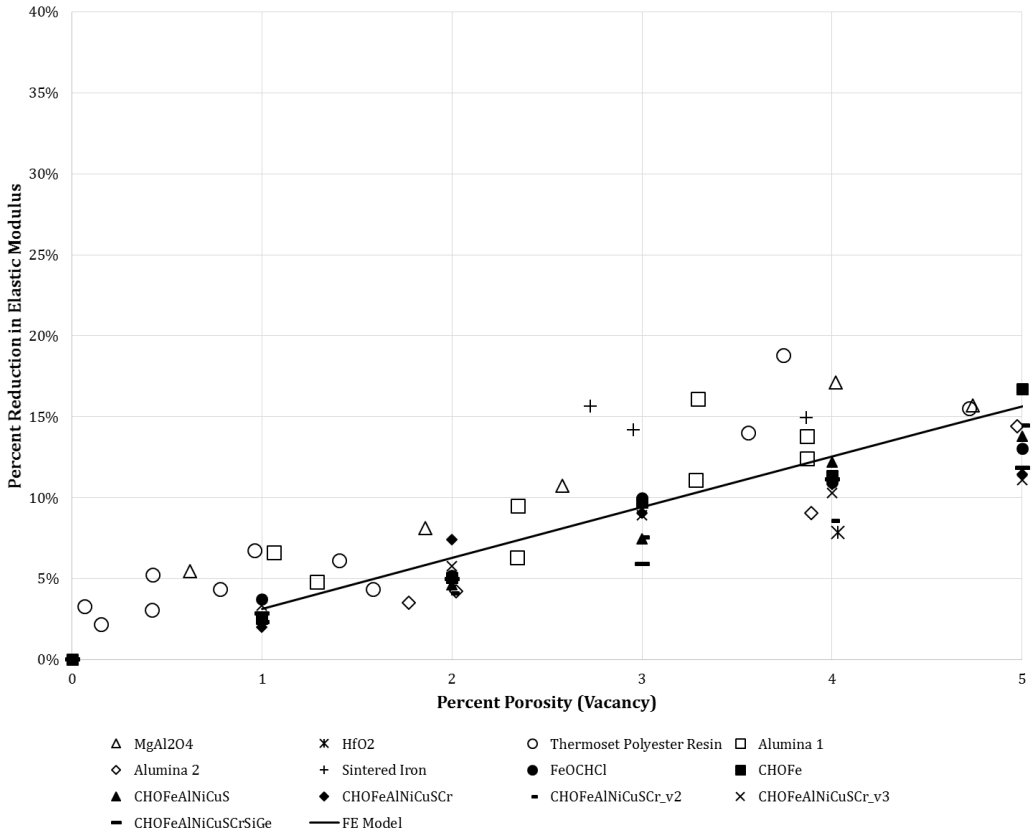

Figure 3-7 - Comparison of ReaxFF for Pure Iron, Morrissey and Nakhla FE Model [1], and Experimental data ($MgAl_2O_4$ [30], HfO_2 [31], Thermoset Polyester Resin [32], Alumina 1 [33], Alumina 2 [34], and Sintered Iron [35]) for the Reduction in Elastic Modulus versus Percent Porosity (Vacancy)

As it can be seen for vacancies of less than 5%, the predicted reduction in modulus, regardless of parameter set, appears to be highly accurate with experimental results and Morrissey and Nakhla's [1] FE model. This trend was unexpected since several of the parameter sets were unable to predict an accurate modulus; however, when the percent reduction is calculated with respect to the zero vacancy modulus calculated for each individual parameter set, the trend is followed closely. On average, Tersoff and ReaxFF follow the trend more closely and this may be possible due to the inclusion of bond order. Table 3-3 shows the average reduction

in modulus of all force fields, experimental results, and Morrissey and Nakhla's [1] FE model.

Table 3-3 - Comparison of Average Reduction from Molecular Dynamics Simulations for Pure Iron, Morrissey and Nakhla's FE Model [1], and Experimental Results [30-35]

Percent Vacancy	Average Reduction per Force Field				Average Reduction from all Force Fields	Average Reduction from Experimental Results [30-35]	FE Model [1]
	EAM	MEAM	Tersoff	ReaxFF			
1	4.6%	5.9%	3.9%	2.8%	4.3%	5.6%	3.1%
2	5.2%	9.4%	8.4%	5.3%	7.1%	8.2%	6.3%
3	9.2%	19.2%	11.5%	8.4%	12.1%	10.7%	9.4%
4	11.8%	21.8%	17.2%	10.8%	15.4%	13.3%	12.5%
5	15.0%	29.5%	18.6%	13.2%	19.1%	15.9%	15.6%

Now that the authors are confident that ReaxFF force field is the most accurate for not only predicting elastic modulus, but also predicting the reduction in modulus as porosity changes, a study on an iron-chromium system can be completed. Unfortunately, due to the limitation of available parameter sets which include iron-chromium bonds, only two parameter sets can be studied – one for EAM (FeCr) and one for ReaxFF (CHOFeAlNiCuSCr).

The ReaxFF parameter set was tested for a pure iron system. As such, the elastic modulus for an iron-chromium system can be compared. Unfortunately, the EAM parameter set requires the presence of chromium atoms and cannot be tested in a pure iron system. Therefore, the accuracy of the predicted modulus with the inclusion of chromium is uncertain. A comparison of the predicted elastic modulus for a zero-vacancy pure iron and iron-chromium system is shown in Table 3-4. It can

be seen that both predicted values for the elastic modulus of iron-chromium differ from the nominal modulus of approximately 200 GPa for 13% chromium stainless steel.

Table 3-4 - Comparison of Predicted Elastic Modulus for Pure Iron and Iron-Chromium

Force Field	Parameter Set	Elastic Modulus Pure Iron (GPa)	Elastic Modulus Iron-Chromium (GPa)	Ref.
EAM	FeCr	-	151.5	[36]
ReaxFF	CHOFeAlNiCuSCr	164.5	175.2	[25]

Figure 3-8 compares the percentage reduction in elastic modulus versus percent vacancy for the iron-chromium system for both parameter sets. Included in the figure are experimental results of reduction in elastic modulus versus percent porosity and Morrissey and Nakhla's [1] FE model which was developed to predict this reduction. As can be seen in Figure 3-8, even though the EAM parameter set is unable to predict an accurate modulus, its predicted percent reduction in modulus due to vacancies is comparable to that predicted by the ReaxFF parameter set. From Table 3-5, it is evident that both parameter sets are accurately capturing the trend of the reduction of elastic modulus as vacancy percentage increases when compared to experimental results and Morrissey and Nakhla's [1] FE model.

Table 3-5 – Comparison of Average Reduction from Molecular Dynamics Simulations for Iron-Chromium, Morrissey and Nakhla's [1] FE Model, and Experimental Results [30-35]

Percent Vacancy	Average Reduction per Force Field		Average Reduction from all Force Fields	Average Reduction from Experimental Results [30-35]	FE Model [1]
	EAM	ReaxFF			
1	1.50%	1.8%	1.6%	5.6%	3.1%
2	4.50%	4.1%	4.3%	8.2%	6.3%
3	6.20%	7.5%	6.8%	10.7%	9.4%
4	13.10%	6.7%	9.9%	13.3%	12.5%
5	15.80%	14.8%	15.3%	15.9%	15.6%

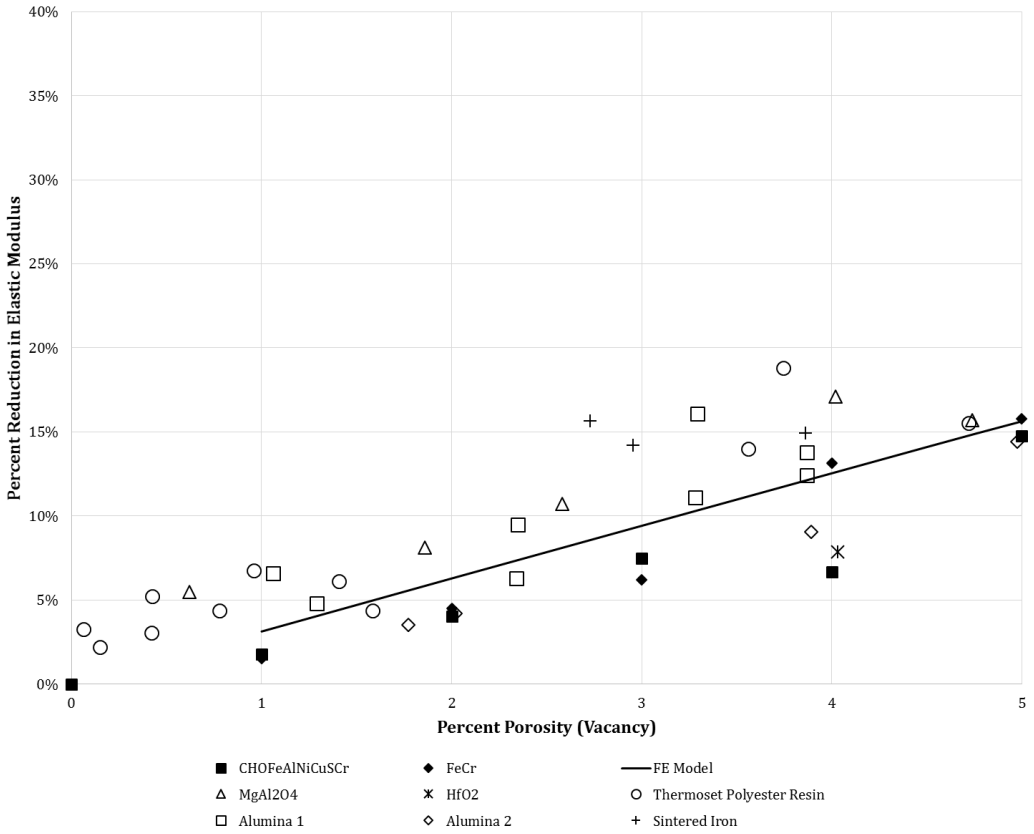

Figure 3-8 - Comparison of EAM and ReaxFF for Iron-Chromium, Morrissey and Nakhla FE Model [1], and Experimental data ($MgAl_2O_4$ [30], HfO_2 [31], Thermoset Polyester Resin [32], Alumina 1 [33], Alumina 2 [34], and Sintered Iron [35]) for the Reduction in Elastic Modulus versus Percent Porosity (Vacancy)

3.5. Conclusion

The authors have shown that atomistic models are capable of predicting accurate elastic modulus with the selection of an appropriate parameter set. In addition, it has been shown that several parameter sets are capable of accurately predicting the reduction in elastic modulus due to vacancy percentage. More accurate predictions will be available as more potentials are parameterized to specific experimental data.

Acknowledgements

The authors are grateful for the financial support from Suncor Inc.

References

1. L.S. Morrissey and S. Nakhla, "A finite element model to predict the effect of porosity on elastic modulus in low porosity materials," Metall and Mat Trans A, vol. 40, pp. 2622-2630, July 2018.
2. S.M. Handrigan, L.S. Morrissey, and S. Nakhla, "A finite element model to study the effect of porosity location on the elastic modulus of a cantilever beam," Manuscript submitted.
3. B. Gong, "Finite element analysis of micro-cantilever beam experiments in UO2", November 2015.
4. A. Rajabpour, L. Seidabadi, and M. Soltanpour, "Calculating the bulk modulus of iron and steel using equilibrium molecular dynamics simulations," Procedia Materials Science, vol. 11, pp. 391-396, 2015.
5. L.S. Morrissey, S.M. Handrigan, S. Subedi, and S. Nakhla, "Atomistic Uniaxial Tension Tests: Investigating various molecular dynamics potentials for their ability to produce accurate stress strain curves," Mol. Sim., in press, doi: 10.1080/08927022.2018.1557333
6. M.S. Daw and M.I. Baskes, "Embedded-atom method: derivation and application to impurities, surfaces, and other defects in metals," Phys. Rev. B, vol. 29 (12), pp. 6443-6453, June 1984
7. B.J. Lee et al., "Second nearest-neighbor modified embedded atom method potentials for bcc transition metals," Phys. Rev. B, vol. 64(18), p. 184102, October 2001
8. J. Tersoff, "New empirical approach for the structure and energy of covalent systems," Phys. Rev. B, vol 37(12), pp. 6991-7000, April 1988

9. A.C.T. van Duin et al., "ReaxFF: a reactive force field for hydrocarbons," Phys. Chem. A, vol. 105(41), pp. 9396-9409, September 2001
10. S. Plimpton, "Fast parallel algorithms for short-range molecular dynamics," Comput. Phys., vol. 117(1), pp. 1-19, March 1995
11. B.D. Jensen, K.E. Wise, G. M. Odegard, "The effect of time step, thermostat, and strain rate on ReaxFF simulations of mechanical failure in diamond, graphene, and carbon nanotube," Comput. Chem., vol. 36, pp. 1587-1596, June 2015
12. R.B. Ross, Metallic Materials Specification Handbook Fourth Edition, Chapman & Hall, London, 1992
13. ASM, ASM Handbook Volume 2: Properties and selection: nonferrous alloys and special-purpose materials, ASM International, October 1990
14. A. Nayar, The metals databook, McGraw-Hill, New York, 1997
15. D. Lide, CRC handbook of chemistry and physics: a ready-reference book of chemical and physical data, 80th Edition, CRC Press Boca Rataon, FL, 1999
16. L. Proville, D. Rodney, and M.-C. Marinica, "Quantum effect on thermally activated glide of dislocations," Nature Materials, vol. 11, pp. 845-849, October 2012
17. M.I. Mendelev et al., "Development of new interatomic potentials appropriate for crystalline and liquid iron," Philosophical Magazine, vol. 83(35), pp. 3977-3994, May 2003
18. H. Chamati et al., "Embedded-atom potential for Fe and its application to self-diffusion on Fe(100)," Surface Science, vol. 600(9), pp. 1793-1803, May 2006
19. E. Asadi et al., "Quantitative modeling of the equilibration of two-phase solid-liquid Fe by atomistic simulations on diffusive time scales," Phys. Rev. B, vol. 91(2), p. 024105, January 2015
20. S.A. Etesami and E. Asadi, "Molecular dynamics for near melting temperatures simulations of metals using modified embedded-atom method," Journal of Physics and Chemistry of Solids, vol. 112, pp. 61-72, January 2018
21. K.O.E. Henriksson, C. Björkas, and K. Nordlund, "Atomistic simulations of stainless steels: a many-body potential for the Fe–Cr–C system." Journal of Physics: Condensed Matter, vol. 25(44), p. 445401, October 2013
22. C. Zou and A.C.T. van Duin, "Investigation of complex iron surface catalytic chemistry using the reaxff reactive force field method," JOM. vol. 64(12), pp. 1426-1437, December 2012
23. M. Aryanpour, A.C.T. van Duin, J.D. Kubicki, "Development of a reactive force field for iron-oxyhydroxide systems," Phys. Chem. A, vol. 114, pp. 6298-6307, May 2010
24. O. Rahaman, A.C.T. van Duin, W.A. Goddard III, and D.J. Doren Development of a ReaxFF reactive force field for glycine and application to solvent effect and tautomerization Journal of Physical Chemistry B 115 (2011), 249-261.
25. Y.K. Shin, H. Kwak, A.V. Vasenkov, D. Sengupta and A.C.T. van Duin Development of a ReaxFF Reactive Force Field for Fe/Cr/O/S and Application to Oxidation of Butane over a Pyrite-Covered Cr2O3 Catalyst ACS Catalysis, 2015, 5 (12), pp 7226-7236

26. C. Zou et al. Molecular dynamics simulations of the effects of vacancies on nickel self-diffusion, oxygen diffusion and oxidation initiation in nickel, using the ReaxFF reactive force field Acta Materialia, Volume 83, 15 January 2015, Pages 102-112
27. F. Tavazza, T.P. Senftle, C. Zou, C.A. Becker and A.C.T van Duin Molecular Dynamics Investigation of the Effects of Tip-Substrate Interactions during Nanoindentation J. Phys. Chem. C, 2015, 119 (24), pp 13580-13589
28. Y. Zheng, S. Hong, G. Psofogiannakis, S. Datta, B. Rayner, A.C.T. van Duin and R. Engel-Herbert Modeling and In-situ Probing of Surface Reactions in Atomic Layer Deposition ACS Appl. Mater. Interfaces, 2017, 9 (18), pp 15848-15856
29. W. P. Mason, Piezoelectric crystals and their application to ultrasonics, New York, Van Nostrand, 1950
30. D.F. Porter, J.S. Reed, and D.L. Iii: J. Am. Ceram. Soc., 1977, vol. 60, pp. 345–49.
31. S.L. Dole, O. Hunter, and F.W. Calderwood: J. Am. Ceram. Soc., 1980, vol. 63, pp. 136–39.
32. K.K. Phani and R.N. Mukerjee: J. Mater. Sci., 1987, vol. 22, pp. 3453–58.
33. F.P. Knudsen: J. Am. Ceram. Soc., 1962, vol. 45, pp. 94–95
34. M. Asmani, C. Kermel, A. Leriche, and M. Ourak: J. Eur. Ceram. Soc., 2001, vol. 21, pp. 1081–86.
35. J.P. Panakkal, H. Willems, and W. Arnold: J. Mater. Sci., 1990, vol. 25, pp. 1397–1402
36. A. Stukowski, B. Sadigh, P. Erhart, and A. Caro, "Efficient implementation of the concentration-dependent embedded atom method for molecular-dynamics and monte-carlo simulations," Model. SImulat. Materi. Sci. Eng., vol. 17(7), July 2009

4. Chapter 4: Summary

The work completed in the above chapters was performed to study the applicability of using computer models to predict the effect of porosity on the elastic modulus of a material. If simulations can be performed, not only is time and money being saved, but the efficacy of analysis is improved. In addition, through the use of simulations, the replicability of the study is increased. The author of this thesis originally discovered the thesis by Gong which inspired the work of Chapter One. Gong's thesis involved the development and analysis of a microscale cantilever. To produce a microscale cantilever, several high CAPEX equipment are required: 1) a nanoindenter with Scanning Electron Microscope (SEM) capable of applying loads on the order of nano-Newtons or displacements at rates of nanometers per second, and 2) a focused-ion beam capable of producing ion beams on the nano-amperes scale. In addition to the costly experimental setup, significant amounts of time were required not only to fabricate the cantilevers, but to also prepare the material for the fabrication of cantilevers and to perform the experiments themselves. To further demonstrate the benefit of simulations, Gong stated that the proper grain sizes were not attainable and as such, the experiments were continued on non-ideal specimens. Each cantilever was to be contained within a single crystal grain but this was not possible, making the cantilever analysis more difficult and less replicable. As a result, the development of simulations to study the effect of microscale porosity on elastic modulus is highly recommended. The use of simulations allows for easy manipulation of the inputs to allow for consistent analysis of a problem. For example, if a new geometry was to be studied (e.g., longer cantilever or different cross-section), then

new samples must be fabricated which is very costly in terms of money and time; however, in a simulation these parameters are easily controlled and manipulated. As well, if various specific porosity values were to be studied, this may not be possible or would result in significant costs to fabricate experimental microcantilevers with the required specific porosity.

As it has been shown in Chapter 2, the author of this thesis has reduced the error in prediction of reduced elastic modulus from +38% to +14% through only the application of correct analysis. No experiments were performed to provide more data, only a 3D FE model was developed through rigorous analysis.

As for Chapter 3, the author has shown that molecular dynamics is capable of accurately predicting the reduction of elastic modulus due to atomistic-scale vacancies, correlating to both experimental data and a FE model from literature. The author does not believe that an experiment of this type could be performed currently, as such, the utilization of simulations has allowed for the analysis to be performed.